NASA SP-240

THE MIXED STATE OF SUPERCONDUCTORS

HUDSON

NATIONAL AERONAUTICS AND SPACE ADMINISTRATION

NASA SP–240

THE MIXED STATE OF SUPERCONDUCTORS

WAYNE R. HUDSON

Lewis Research Center, Cleveland, Ohio

Scientific and Technical Information Division
OFFICE OF TECHNOLOGY UTILIZATION 1970
NATIONAL AERONAUTICS AND SPACE ADMINISTRATION
Washington, D.C.

For sale by the Superintendent of Documents,
U.S. Government Printing Office, Washington, D.C. 20402
Price 40 cents
Library of Congress Catalog Card Number 79–606936

PREFACE

The purpose of this book is to review the present knowledge of the mixed state of superconductivity. It is the hope of the author that this review will be helpful to persons unfamiliar with the subject. The fundamentals are discussed in detail to provide sufficient background for the understanding of more recent developments. The emphasis is on the experimental and theoretical aspects of flux creep and flux flow. The thermal properties of the mixed state have not been discussed.

This publication was originally prepared in partial fulfillment of the requirements for a Master of Science degree at John Carroll University, Cleveland, Ohio.

CONTENTS

INTRODUCTION

The discussion begins with a review of the fundamental properties of superconductivity. Then the Ginzburg-Landau equations are described and Abrikosov's solution is discussed. The vortex state is compared to a laminar state to determine which state is energetically more favorable. The experimental evidence that substantiates the vortex state is given. The results of tube magnetization experiments are presented, and the flux creep theory is derived. The flux flow models of Bardeen-Stephen and Nozieres-Vinen are compared with each other and with the experimental evidence. Three models for the viscosity coefficients are presented. Finally, the rigidity of the Abrikosov structure and the possible flux line pinning mechanisms are mentioned.

Zero Resistance Effect

In 1908 Kamerlingh Onnes liquefied helium for the first time. Electrical resistivity was not very well understood and Onnes decided to make use of his liquid helium capability to study the dependence of resistivity on temperature. He believed that if he could obtain a metal in a pure enough condition its resistivity would approach zero at absolute zero. For this reason he chose mercury. Figure 1 shows the results obtained by Onnes.

Onnes found that the resistivity dropped very abruptly to an unmeasurably small value at a temperature just slightly above the normal boiling point of helium (ref. 1). This transition temperature is now called the critical temperature T_c. Initially Onnes explained that this result occurred because of the purity of the mercury. He discarded this conclusion when he found that the resistivity of mercury disappeared even when impurities were added. The addition of impurities did, however, increase the temperature span over which the resistivity dropped to zero. The sharpness of the transition and its relative insensitivity to alloying forced Onnes to conclude that mercury had undergone a very fundamental change to a new electronic state. He named the new state the superconducting state.

The discovery of the superconducting state opened a whole new area of research. One obvious question was how many other substances exhibit the zero resistance effect. As of 1963, more than 900 superconducting materials have been found (ref. 2). Among the known superconducting materials are metals, semiconductors, alloys, and compounds.

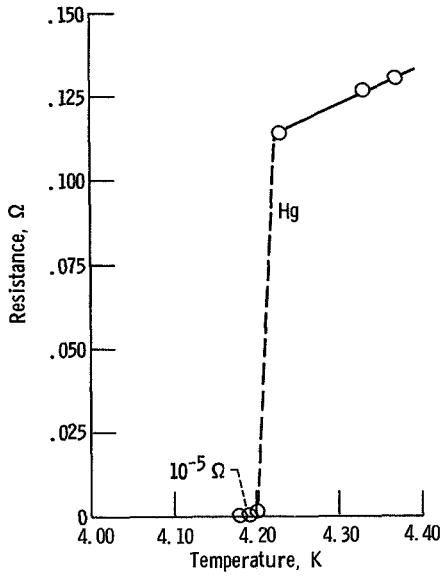

FIGURE 1.—Resistance of mercury plotted against absolute temperature (ref. 105).

The new electronic state was also probed experimentally in many ways. Onnes (refs. 3 and 4) discovered that if an electric current through a superconductor exceeds a critical value the material becomes resistive. He also discovered (ref. 5) that if a magnetic field is applied to a superconductor the resistance returns when the field exceeds a particular critical value H_c. The detailed nature of the magnetic transition became known somewhat later (refs. 6 and 7). The critical magnetic field was found to be temperature dependent. In many materials the temperature dependence is described fairly well by

$$H_c = H_o\left[1-\left(\frac{T}{T_c}\right)^2\right] \tag{1}$$

where H_o is the critical field at absolute zero. Some experimentally determined critical field against temperature curves may be found in appendix A. In the region above the critical curve the material is in the normal state, and in the region below the curve it is in the superconducting state. It was suggested by Silsbee (ref. 8) that the critical current and the critical magnetic field are related. Silsbee's hypothesis is that the critical current is the current which generates a self field equal to the critical magnetic field.

The superconducting state is very sensitive to impurities and deformations. Figure 2 shows the changes that occur in the resistive

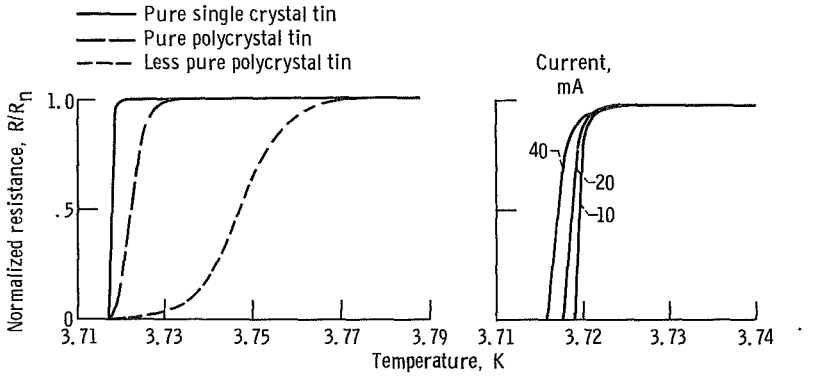

(a) Influence of physical properties of the samples.

(b) Influence of measuring current.

FIGURE 2.—Reduced resistance against absolute temperature (ref. 102).

transition which depend on the sample condition and the measuring current. These measurements, which were made by deHaas and Voogd (ref. 9), showed that the transition could take place in a temperature span as small as 0.001 K. The specific heat of a superconductor changes discontinuously at the critical temperature, and the thermoelectric power of superconductors is equal to zero.

Since superconductivity was discovered, various researchers have attempted to measure a resistance in the superconducting state. The early potentiometric measurements of Onnes were accurate enough to show that resistivity in the superconducting state was 10^{-6} less than the normal state resistivity. Since then various investigators have been able to put an upper bound on the resistivity by inducing a current in a ring of superconducting material and measuring its decay. Onnes was the first to use the method. Grassman (ref. 10) reported a resistivity of less than 10^{-12} of the normal state value. Recently File and Mills (ref. 11) have performed experiments where the decay time of a niobium zirconium (NbZr) solenoid was measured. They found that the decay time of the persistent currents must be greater than 100 000 years.

Meissner Effect

In 1933, Meissner and Ochsenfeld (ref. 12) discovered an abrupt change in the apparent magnetization of tin as it was cooled below the transition temperature. The original purpose of their experiment was to determine if the current in a superconductor flowed on the surface or in the bulk. The experimental scheme was to measure the magnetic

field in the vicinity of a U-shaped current-carrying wire. They hoped to be able to distinguish between the two modes of current flow by measuring small differences in the magnetic field. What they found instead was that the magnetic field surrounding the wire increased sharply when their sample became superconducting.

Later experiments showed that the magnetic field is totally expelled from the bulk of a superconductor when the magnetic field is less than the critical field. The applied magnetic field H_a is excluded by superconducting surface currents. If these currents are represented by an equivalent magnetization, the Meissner effect can be shown graphically by plotting magnetization as a function of applied magnetic field (fig. 3). Below H_c there is no magnetic field inside the superconductor and the magnetic flux density B equals zero. Therefore $B=H_a+4\pi M$ becomes $H_a=-4\pi M$. Above H_c the superconductor can no longer expel the magnetic field and the sample undergoes a transition to the normal state.

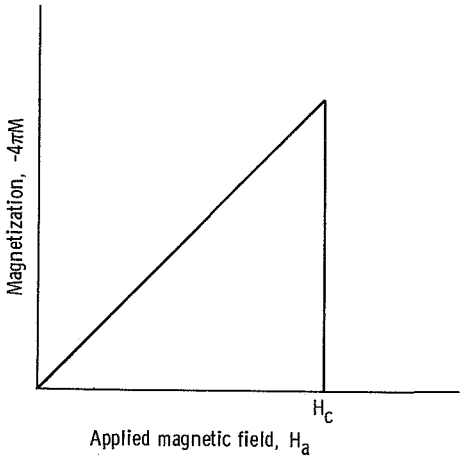

FIGURE 3.—Ideal magnetization against applied magnetic field for superconductor. Below H_c superconductor is perfectly diamagnetic, $H_a=-4\pi M$.

The Meissner effect may be complicated by the sample geometry and the orientation of the magnetic field with respect to the sample. These effects, called demagnetization effects, are discussed in detail in references 13 and 14. Basically, figure 3 would be obtained only for an infinitely long cylindrical sample with the magnetic field paralled to its axis. In this geometry the magnetic field is paralled to the internal magnetization. The critical field H_c is defined for this geometry. Any other geometry exhibits a lower value of critical field. When the sample

geometry or the sample orientation with respect to the magnetic field is such that magnetic field penetrates the sample below H_c, the sample is said to be in the intermediate state. The intermediate state has been optically observed using an experimental technique that takes advantage of the Faraday rotation effect (ref. 15). Some pictures taken by Faber (ref. 16) are shown in appendix B. These particular pictures are of an aluminium plate. The dark areas are superconducting regions. The pictures show that the intermediate state is composed of alternating normal and superconducting regions which are laminar-like in appearance. The width of the superconducting laminae are seen to decrease with magnetic field. The size of the normal and superconducting laminae varies because the total magnetic flux through the sample must be equal to the applied flux, and the magnetic field in the normal regions is H_c.

London Equation and Penetration Depth

Prior to the discovery of the Meissner effect, Becker, Heller, and Sauter (ref. 17) had analyzed the electric and magnetic properties of a "perfect conductor" (zero resistance, but no Meissner effect). Their analysis predicts that any magnetic field in a material when it becomes superconducting will be trapped inside the sample. This prediction was contradicted by the Meissner effect.

F. London and H. London (ref. 18) postulated a fundamental contradiction between the Becker-Heller-Sauter prediction and the Meissner effect. They proposed that in superconductors

$$\boldsymbol{J}(r) = -\frac{n_s e^2}{mc}\boldsymbol{A} \tag{2}$$

where $\boldsymbol{J}$ is the current density, n_s the number of superconducting electrons, e the charge of an electron, m the mass of an electron, c the speed of light, and $\boldsymbol{A}$ the magnetic vector potential. Then, starting with the Maxwell equation

$$\nabla \times \boldsymbol{H} = \frac{4\pi}{c}\boldsymbol{J} \tag{3}$$

and taking the curl of both sides of both the London and the Maxwell equations yields

$$\nabla \times \boldsymbol{J} = -\frac{n_s e^2}{mc}(\nabla \times \boldsymbol{A}) = -\frac{n_s e^2}{mc}\boldsymbol{H} \tag{4}$$

and

$$\nabla \times \nabla \times \boldsymbol{H} = \frac{4\pi}{c}(\nabla \times \boldsymbol{J}) \tag{5}$$

Substituting equation (4) into equation (5) results in

$$\nabla \times \nabla \times \boldsymbol{H} = -4\pi \frac{n_s e^2}{mc^2} \boldsymbol{H} \tag{6}$$

For a magnetic field parallel to the surface of a superconducting half space, equation (6) is reduced to one dimension and has solutions of the form

$$\boldsymbol{H} = \boldsymbol{H}_a e^{-x/\lambda_L} \tag{7}$$

where $\lambda_L = (mc^2/4\pi n_s e^2)^{1/2}$ and $\boldsymbol{H}_a$ is the applied magnetic field. The x coordinate is perpendicular to the surface of the superconducting region. This result agrees with the Meissner effect because it predicts that in the bulk the magnetic field is essentially zero. The parameter λ_L, which is called the London penetration depth, is the distance from the surface of a semi-infinite slab to the point where $H = H_a/e$. The shielding currents mentioned earlier reside primarily within a few penetration depths of a sample's surface. A typical value for λ_L is about 500 Å at 0 K. The penetration depth is relatively constant except near the critical temperature where n_s goes to zero. Table I (p. 65) contains measurements of the penetration depth for several materials.

Mixed State

In 1934 and 1935 Mendelssohn and his coworkers at Oxford observed some rather disconcerting experimental results on superconducting alloys. They were investigating the Meissner effect in various materials: mercury (Hg), lead (Pb), tin (Sn), tantalum (Ta), tin bismuth (SnBi), lead bismuth (PbBi), and lead telluride ($PbTl_2$). They sought to observe the sharp and reversible changes in the specific heat of superconductors, which were predicted by the thermodynamic treatments of Gorter and Casmir (refs. 19 and 20). Gorter and Casmir assumed that the Gibbs free energy of a superconductor G_s was related to the free energy of a normal conductor G_n by

$$G_n = G_s(0) + \frac{H_c^2}{8\pi} \tag{8}$$

and had a magnetic field dependence of

$$G_s(H) = G_s(0) + \frac{H^2}{8\pi} \tag{9}$$

From these assumptions they derived a discontinuity in the specific heat. Keeley and Mendelssohn (ref. 21) found that only mercury had a reversible magnetization. Tin and lead exhibited some hysteresis; tantalum was found to have even more. In addition, the alloys were described by Mendelssohn as being completely irreversible. There were other differences between the experimental results for alloys and the same results on elements. The empirical fact observed for elements, that the resistance and magnetic induction go to zero at the same magnetic field value, was not found to be true for alloys. Gorter's prediction of a specific heat discontinuity had been observed by Mendelssohn and Moore in tin (ref. 22) and by Keesom and Kok (ref. 23) in thallium. Their specific heat measurements were consistent with each other and with Gorter's prediction. But when Mendelssohn and Moore (ref. 24) investigated the specific heat of $PbTl_2$, which they estimated should have a large specific heat discontinuity, they found the result shown in figure 4. No indication of a discontinuity was observed. These results strongly suggested that

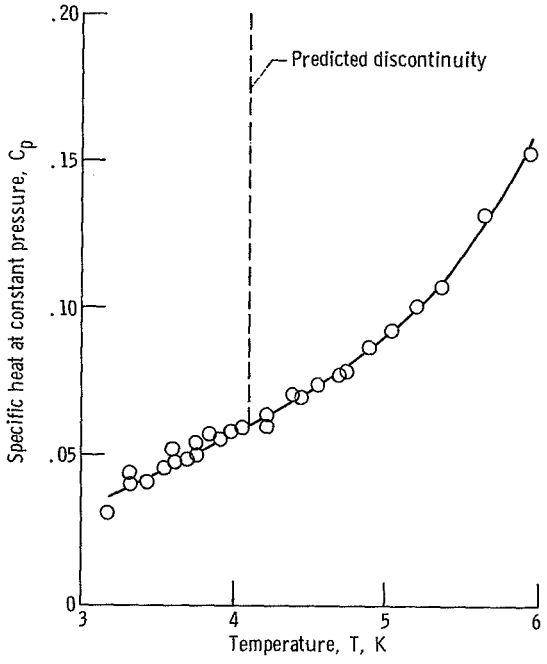

FIGURE 4.—Specific heat C_p of $PbTl_2$ against absolute temperature (ref. 24).

a fundamental difference exists between the superconducting properties of pure metals and alloys.

It has since been shown (ref. 25) that even if the magnetization as a function of applied magnetic field curves of alloys are completely reversible they are fundamentally different from figure 3. Figure 5 shows the magnetization that characterizes most alloys. Up to H_{c1} the magnetic field is completely excluded, but between H_{c1} and H_{c2} the magnetic field inside the material increases until the material becomes completely normal at H_{c2}. Materials which exhibit this type of magnetization curve are called type II superconductors. Superconductors that have a magnetization curve as shown in figure 3 are called type I. When the magnetic field of a type II superconductor is between H_{c1} and H_{c2} the superconductor is said to be in the mixed state. The mixed state is distinguished from the intermediate state in that it is not a geometry effect, the mixed state is rather an independent equilibrium state of the system.

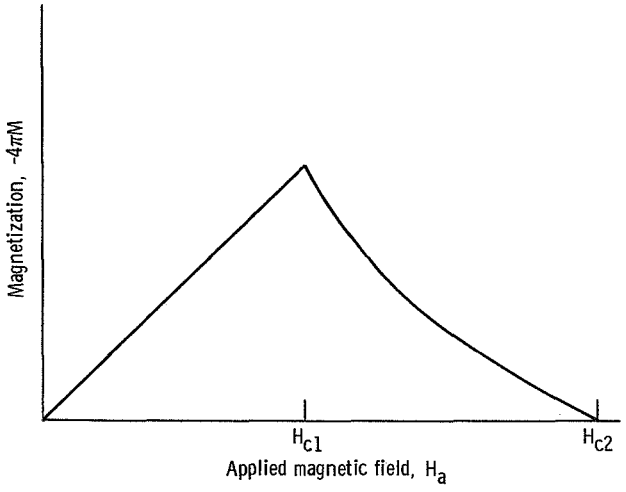

FIGURE 5.—Magnetization against applied magnetic field for type II superconductor.

Figure 6 shows how the magnetization is affected by alloying. Starting with pure lead, which is a type I superconductor, increasing amounts of indium are added. The resulting alloy is a type II superconductor. As the percent of indium in the alloy is increased, H_{c1} decreases and H_{c2} increases. The table accompanying the figure shows how the ratio of H_{c2} to H_{c1} varies.

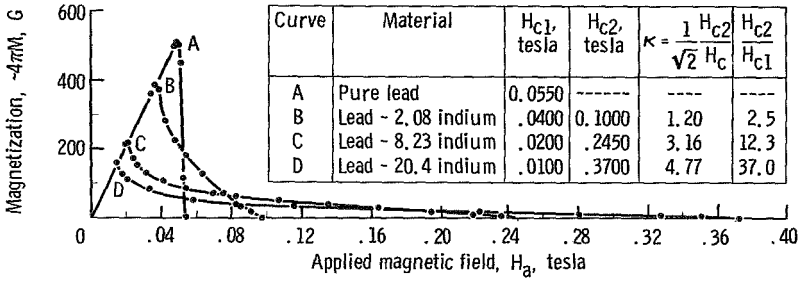

Curve	Material	H_{c1}, tesla	H_{c2}, tesla	$\kappa = \frac{1}{\sqrt{2}} \frac{H_{c2}}{H_c}$	$\frac{H_{c2}}{H_{c1}}$
A	Pure lead	0.0550	------	----	----
B	Lead - 2.08 indium	.0400	0.1000	1.20	2.5
C	Lead - 8.23 indium	.0200	.2450	3.16	12.3
D	Lead - 20.4 indium	.0100	.3700	4.77	37.0

FIGURE 6.—Effect of alloying on magnetization curve of lead (ref. 105). Key shows variation of H_{c1}, H_{c2}, κ, and H_{c2}/H_{c1} with alloying; thermodynamic critical field, $H_c = 0.0550$ tesla.

Bardeen-Cooper-Schrieffer Theory and Coherence Length

The modern era of superconductivity began in 1950 when Frohlich (ref. 26) suggested that superconductivity might be explained by phonon coupling between electrons. Frohlich was able to predict that the dependence of the critical temperature on the isotropic mass was $T_c \propto M^{-1/2}$. About the same time, this relation was discovered experimentally in mercury (refs. 27 and 28). These results strongly suggested that superconductivity results from an electron-lattice interaction. In 1957, Bardeen, Cooper, and Schrieffer (B.C.S.) put forth a theory based on the electron-phonon interaction suggested by Frohlich (refs. 29 and 30). The B.C.S. theory proposes that the interaction occurs between electrons with opposite momenta and spin.

The interaction may be visualized as follows. An electron moves through the lattice attracting the positive lattice toward it. A second electron can be attracted to the deformed region by the excess of positive charge there. This effectively attractive interaction between the two electrons results in an energy gap between an electron in the B.C.S. ground state and the Fermi level. The energy gap Δ, which is related to the critical temperature by $\Delta \propto k_B T_c$, leads to the critical fields and the thermal properties mentioned earlier. The attractive force between the electrons extends over a distance which is called the coherence length ξ. The coherence length can also be interpreted as the distance over which the energy gap Δ cannot change drastically. The B.C.S. theory results in the following fundamental relation at $T=0$ K between the energy gap and the coherence length ξ_o:

$$\xi_o = \frac{2\hbar v_f}{\pi \Delta_o} \sim 10^{-4} \text{ cm} \tag{10}$$

where v_f is the Fermi velocity and $\hbar$ is Planck's constant divided by 2π. Some typical values of the coherence length are exhibited in appendix C. Prior to the formulation of the B.C.S. theory, Pippard (ref. 31) had predicted that a characteristic length like the coherence length must exist. He further proposed that the coherence length is related to the mean free path Λ by the equation

$$\frac{1}{\xi}=\frac{1}{\xi_o}+\frac{1}{\Lambda} \tag{11}$$

Two limitations of the B.C.S. theory are first that it does not predict the mixed state of type II superconductors and second that it does not apply to current carrying superconductors.

Abrikosov's Analysis of the Mixed State

Abrikosov (ref. 32) showed that in the mixed state the magnetic field penetrates the superconductor in discrete flux tubes which are enclosed in vortices of superconducting electrons. Each tube of flux contains a flux quantum φ_o equal to 2.07×10^{-15} meter squared tesla. The existance of the flux quantum was originally predicted by London (ref. 33, p. 151; see also ref. 13, p. 32). Figure 7 shows the spacial variations of the current density of the vortex $|J|$, the magnetic field H, and the energy gap Δ in the region near a tube. Abrikosov's analysis gives the following relations between H_{c1}, H_{c2}, and H_c:

$$H_{c1}=H_c\left(\frac{\xi}{\lambda}\right)\left[\ln\left(\frac{\lambda}{\xi}\right)-0.27\right] \tag{12}$$

and

$$H_{c2}=\sqrt{2}\left(\frac{\lambda}{\xi}\right)H_c \tag{13}$$

These results suggest that the relationship between the penetration depth λ and the coherence length ξ determines whether a superconductor is type I or II. If $\lambda/\xi>1/\sqrt{2}$ then equation (13) implies that $H_{c2}>H_c$ and the superconductor must be type II. Equation (12) predicts that for a type II superconductor, $H_{c1}<H_c$. In figure 6, H_{c1} decreased with alloying and H_{c2} increased. This figure can now be understood in terms of equations (11) to (13). Alloying lead with indium reduces the mean free path and equation (11) predicts that ξ will also be reduced. If ξ is reduced while λ remains constant, then equations (12) and (13) predict the experimental observation in figure 6. The ratio of λ to ξ is called the Ginzburg-Landau kappa κ.

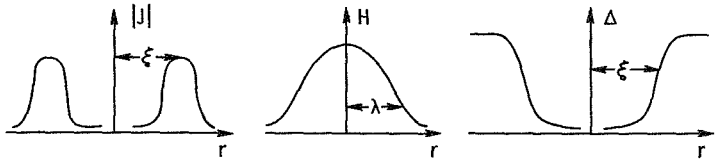

FIGURE 7.—Spatial variations of $|J|$, H, and Δ that make up an Abrikosov vortex. Energy gap Δ is proportional to n_s.

GINZBURG-LANDAU THEORY

The Ginzburg-Landau (G.L.) theory (ref. 34) is a thermodynamic approach to superconductivity. Ginzburg and Landau postulated that an additional term needed to be added to the Gibbs free energy $G_s(H)$ (given by eq. (9)). The new term is needed to incorporate the kinetic energy $(\nabla\psi)^2$ that results when n_s vary spatially. In the Ginzburg-Landau formulation, ψ is called the order parameter, but it is now known to correspond to the wave function of a pair of superconducting electrons. The number density of superconducting electrons n_s is proportional to $|\psi|^2$. To keep their theory gage-invariant, Ginzburg and Landau included a gradient term and a constant term. The total Gibbs free energy is

$$G_s(H)=G_s(0)+\frac{H^2}{8\pi}+\frac{1}{2m}\left|\left(-i\hbar\nabla\psi\frac{2e}{c}A\psi\right)\right|^2 \tag{14}$$

The $G_s(0)$ term can be written as a function of ψ utilizing the Landau-Lifshitz general theory of second-order phase transitions (ref. 35). The Landau-Lifshitz theory states that near the transition temperature the Gibbs free energy can be expressed as a series expansion in $|\psi|^2$. Therefore,

$$G_s(0)=G_n(0)+\alpha(T)|\psi|^2+\frac{\beta(T)}{2}|\psi|^4+\ldots \tag{15}$$

The minimum value of $G_s(0)$ corresponds to the equilibrium value of $|\psi|^2$. Both $\alpha(T)$ and $\beta(T)$ are temperature-dependent coefficients. The minimum of $G_s(0)$ is obtained by taking the partial derivative of $G_s(0)$ with respect to $|\psi|^2$ and setting it equal to zero:

$$\frac{\partial G_s}{\partial|\psi|^2}=\alpha(T)+\beta(T)|\psi|^2=0 \tag{16}$$

$$|\psi|^2=-\frac{\alpha(T)}{\beta(T)} \tag{17}$$

Equation (18) is obtained by substituting $|\psi|^2$ into equation (15) and comparing the result with equation (8):

$$\frac{\alpha^2(T)}{2\beta(T)}=\frac{H_c^2}{8\pi} \tag{18}$$

Near T_c, if it is assumed that

$$\left.\begin{aligned}\alpha(T)&=(T_c-T)\left(\frac{\partial\alpha}{\partial t}\right)_{T=T_c}\\ \text{and}\qquad\qquad\\ \beta(T)&=\beta(T_c)\equiv\beta_c\end{aligned}\right\} \tag{19}$$

then substituting for $\alpha(T)$ and $\beta(T)$ in equation (18) results in

$$H_c^2=\frac{4\pi(T_c-T)^2}{\beta_c}\left(\frac{\partial\alpha}{\partial t}\right)^2_{T=T_c} \tag{20}$$

This is consistent with experimental results. Near T_c, H_c is usually found to be proportional to T_c-T. This agreement tends to validate the assumptions in equation (19).

The Ginzburg-Landau equations can be derived by integrating equation (14) over the volume of the superconductor and then minimizing the result with respect to both ψ and A. This can be done using the Euler method (ref. 36). The general results (ref. 34) are

$$\left|\left(\frac{i\nabla}{\kappa}+\boldsymbol{A}\right)\right|^2\psi=\psi-\psi|\psi|^2 \tag{21}$$

and

$$\nabla^2\boldsymbol{A}=|\psi|^2\boldsymbol{A}+\frac{i}{2\kappa}(\psi^*\nabla\psi-\psi\nabla\psi^*) \tag{22}$$

Both equations (21) and (22) have been reduced to a standard dimensionless form where lengths are normalized to λ, magnetic field is normalized to $\sqrt{2}H_c$, and ψ is normalized to $\psi_{H=0}$. The Ginzburg-Landau parameter κ equals $\sqrt{2}(e/\hbar c)H_c\lambda^2$. London's equation (eq. (2)) is obtained from equation (22) in the limit of low magnetic field, as $H\rightarrow 0$, because $\psi=\psi_o$ and $\nabla\psi=0$.

The Ginzburg-Landau equations have been derived from the microscopic theory of Bardeen, Cooper, and Schrieffer by Gorkov (ref. 37). These equations can be classified as coupled nonlinear equations in ψ and A. Because of their inherent complexity they have been solved primarily for one-dimensional problems. A partial listing of the problems to which they have been applied includes the properties of super-

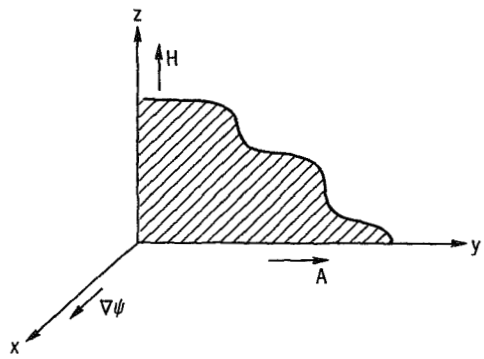

FIGURE 8.—Infinite superconducting half space.

conductors at high fields, the critical fields of thin films, supercooling in type I superconductors, the dependence of penetration depth on field, and the calculation of the interphase boundary energy.

It is informative at this point to derive the Ginzburg-Landau equations for a simple one-dimensional model. First, insight is gained into the Ginzburg-Landau equations. Second, the very important prediction that there are two distinct kinds of superconductors can be readily derived from the solutions. The pedagogical development which follows is in large part due to Newhouse (ref. 14). Consider an infinite superconducting half space $x < 0$ (fig. 8). If H is in the z-direction and A is in the y-direction, then $\boldsymbol{A} = A(x)$ and $\psi = \psi(x)$. Therefore, $\boldsymbol{H} = d\boldsymbol{A}/dx$. Because $\nabla\psi$ is in the x-direction, $\boldsymbol{A}\cdot\nabla\psi = 0$. Incorporating these facts into the total Gibbs free energy equation (eq. (14)) yields

$$G_s(H) = G_s(0) + \frac{1}{8\pi}\left(\frac{dA}{dx}\right)^2 + \frac{1}{2m}\left[\hbar^2\left(\frac{d\psi}{dx}\right)^2 + \left(\frac{2eA}{c}\,\psi\right)^2\right] \tag{23}$$

The corresponding Euler equations (ref. 36) are

$$\frac{\partial G_s(H)}{\partial \psi} - \frac{d}{dx}\left(\frac{\partial G_s(H)}{\partial \psi_x}\right) = 0 \tag{24}$$

and

$$\frac{\partial G_s(H)}{\partial A} - \frac{d}{dx}\left(\frac{\partial G_s(H)}{\partial A_x}\right) = 0 \tag{25}$$

where $\psi_x = \partial\psi/\partial x$ and $A_x = \partial A/\partial x$. When ψ, ψ_x, A, and A_x are regarded

as independent variables, equations (24) and (25) can be evaluated by taking the appropriate derivatives of equation (23). The result is the Ginzburg-Landau equations for this geometry:

$$\frac{d^2\psi}{dx^2}=\frac{m}{\hbar^2}\frac{\partial G_s(0)}{\partial\psi}+\left(\frac{2eA}{\hbar c}\right)^2\psi \tag{26}$$

and

$$\frac{d^2A}{dx^2}=\frac{16\pi e^2}{mc^2}\psi^2A \tag{27}$$

To completely determine equation (26), $\partial G_s(0)/\partial\psi$ must be evaluated exactly. The $\alpha(T)$ and $\beta(T)$ in equation (15) can be expressed in terms of experimentally observable parameters. Starting with the Maxwell equation,

$$\nabla\times\boldsymbol{H}=\frac{4\pi}{c}\boldsymbol{J} \tag{28}$$

If $\nabla\cdot\boldsymbol{A}=0$ then $\nabla\times\nabla\times\boldsymbol{A}=-\nabla^2\boldsymbol{A}=-d^2\boldsymbol{A}/dx^2$ in one dimension, and

$$\frac{d^2A}{dx^2}=-\frac{4\pi}{c}J \tag{29}$$

Substituting the result into equation (27) yields

$$J=-\frac{4e^2}{mc}\psi^2A \tag{30}$$

Equation (31) is obtained by substituting equation (17) into equation (30) and comparing with the London equation (eq. (2)):

$$\frac{\alpha(T)}{\beta(T)}=-\frac{m}{4\pi}\left(\frac{c}{2e\lambda_L}\right)^2 \tag{31}$$

The penetration depth $\lambda_L=(mc^2/4\pi n_se^2)^{1/2}$ was defined by equation (7). For convenience in writing and reading the equations that follow, $\Gamma=(2e\lambda_L/c)^2$. Expressions for $\alpha(T)$ and $\beta(T)$ are obtained by combining equation (31) with equation (18) and solving for $\alpha(T)$ and $\beta(T)$:

$$\left.\begin{aligned} \alpha(T) &= -\frac{H_c^2}{m}\,\Gamma \\ \text{and} \qquad \beta(T) &= \frac{4\pi H_c^2}{m^2}\,\Gamma^2 \end{aligned}\right\} \tag{32}$$

Substituting into the Gibbs free energy equation (eq. (15)) yields

$$G_s(0) = G_n(0) + \left(-\frac{H_c^2}{m}\,\Gamma\right)\psi^2 + \left(\frac{2\pi H_c^2}{m^2}\,\Gamma^2\right)\psi^4 \tag{33}$$

Taking the derivative gives

$$\frac{\partial G_s(0)}{\partial \psi} = \frac{\partial G_n}{\partial \psi} - \frac{2H_c^2}{m}\,\Gamma\psi + \frac{8\pi H_c^2}{m^2}\,\Gamma^2\psi^3 \tag{34}$$

If $\partial G_n(0)/\partial x = 0$ is substituted into equation (34) and the result is substituted into equation (26),

$$\frac{d^2\psi}{dx^2} = \frac{\kappa^2}{\lambda_L^2}\left[-\left(1 - \frac{A^2}{2H_c^2\lambda_L^2}\right)\psi + \frac{\psi^3}{\psi_o^2}\right] \tag{35}$$

where

$$\left.\begin{aligned} \kappa &= \frac{2\sqrt{2}eH_c\lambda_L^2}{\hbar c} \\ \text{and} \qquad \psi_o^2 &= \frac{m}{4\pi}\left(\frac{c}{2e\lambda_L}\right)^2 \end{aligned}\right\} \tag{36}$$

Equation (35) can be put in the same form as the Schroedinger equation for a simple harmonic oscillator with real periodic solutions if $H \geqslant H_c$ and $\psi_o \gg \psi$:

$$\frac{d^2\psi}{dx^2} = -\frac{\kappa^2}{\lambda_L^2}\left(1 - \frac{H^2x^2}{2H_c^2\lambda_L^2}\right)\psi \tag{37}$$

The solutions are real and periodic only if

$$\frac{H}{H_c} = \frac{\kappa\sqrt{2}}{2n+1} \qquad n = 0,\ 1,\ 2,\ \ldots \tag{38}$$

The maximum value of H/H_c occurs when $n = 0$. Therefore, the lowest magnetic field a superconducting material can be in without the nucleation of superconductivity is

$$H_{c2}=\kappa\sqrt{2}H_c \tag{39}$$

From this equation it can be seen that at $\kappa > 1/\sqrt{2}$ the upper critical field H_{c2} becomes greater than H_c. This range of κ corresponds to type II superconductivity. The value $\kappa=1/\sqrt{2}$ is then the dividing point between types I and II superconductors.

MIXED STATE, VORTEX OR LAMINAR?

The theoretical confirmation of type II superconductors from the Ginzburg-Landau theory raises the question of the nature of the mixed state. What form does the flux inside the superconductor take? Historically two models were proposed, the laminar model (ref. 25) and the vortex model (ref. 32). In both models the mixed state is thought of as consisting of normal regions, where most of the flux resides, and superconducting regions, where London's equation is obeyed. In the laminar model the normal regions are plane laminae of thickness 2ξ. The vortex model proposes that the normal regions, often called normal cores, are cylinders of radius ξ. The laminar model was proposed because laminae have been observed experimentally (appendix B) in the intermediate state of type I superconductors. The vortex model resulted from Abrikosov's solution of the Ginzburg-Landau equations.

Abrikosov Solution of Ginzburg-Landau Equations

The most important solution of the Ginzburg-Landau equations from the standpoint of providing insight into the mixed state was found by Abrikosov (ref. 32). Onsager (ref. 38) and Feynman (ref. 39) predicted that vortices should exist in superfluid helium. Abrikosov became convinced that vortices of current must exist in a superconductor. He therefore set out to find a doubly periodic solution to the Ginzburg-Landau equations. He started out with very restrictive assumptions. He assumed that the superconductor extends throughout all space. The superconductor is assumed to be near T_c, which implies that $|\psi|^2 \ll 1$. The magnetic field inside the superconductor H is set equal to the applied field H_a. It is assumed that H_a is just slightly less than H_{c2}. It is further assumed that $\kappa > 1/\sqrt{2}$.

Abrikosov first sought to solve equation (21). If $\boldsymbol{H}_a$ is in the z-direction and $\boldsymbol{A}$ is directed along the y-axis, then

$$\left.\begin{aligned}\boldsymbol{H}&=\boldsymbol{H}_a\\ \boldsymbol{A}&=\boldsymbol{H}_a x\end{aligned}\right\} \tag{40}$$

Substituting this result for A into equation (21), ignoring the $\psi|\psi|^2$ term, and taking $\psi=\psi(x)$ give

$$\frac{\partial^2\psi}{\partial x^2}-\kappa^2(-H_a^2x^2+1)\psi=0 \tag{41}$$

This equation has solutions of the form

$$\psi=e^{-\frac{\kappa^2x^2}{2}} \tag{42}$$

This simple analysis lead Abrikosov to a less restrictive solution of equation (21):

$$\left.\begin{aligned}\Psi&=\sum_{n=-\infty}^{\infty}C_ne^{iknx}\psi_n(x)\\ \psi_n(x)&=e^{\left[-\frac{\kappa^2}{2}\left(x-\frac{kn}{\kappa^2}\right)^2\right]}\end{aligned}\right\} \tag{43}$$

where k and C_n are arbitrary constants. Substituting this solution into equation (22) and solving for A yield

$$A=H_ax-\frac{1}{2\kappa}\int|\psi|^2dx \tag{44}$$

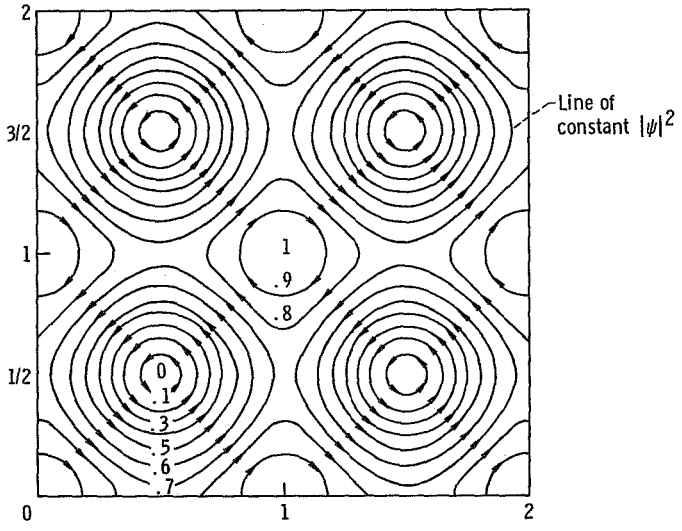

FIGURE 9.—Plot shows that for Abrikosov's solution $|\psi|^2$ has the symmetry of a square lattice. Spatial dimension is normalized to lattice constant, distance between adjacent vortex centers (ref. 32).

Then equation (44) is substituted into equation (21) and the $\Psi|\Psi|^2$ term is included. If the resulting solutions are forced to be periodic and the Gibbs free energy is minimized, the spatial variation of $|\psi|^2$ can be calculated. The solution $|\psi|^2$ is found to have the symmetry of a square lattice in a plane perpendicular to the field direction (fig. 9). At the center of each vortex ψ vanishes and $H=H_a$ at these points. The lines correspond to constant $|\psi|^2$ and constant H. Subsequently, Kleiner, Roth, and Autler (ref. 40) and Matricon (ref. 41) showed that a triangular lattice has a slightly lower energy (fig. 10).

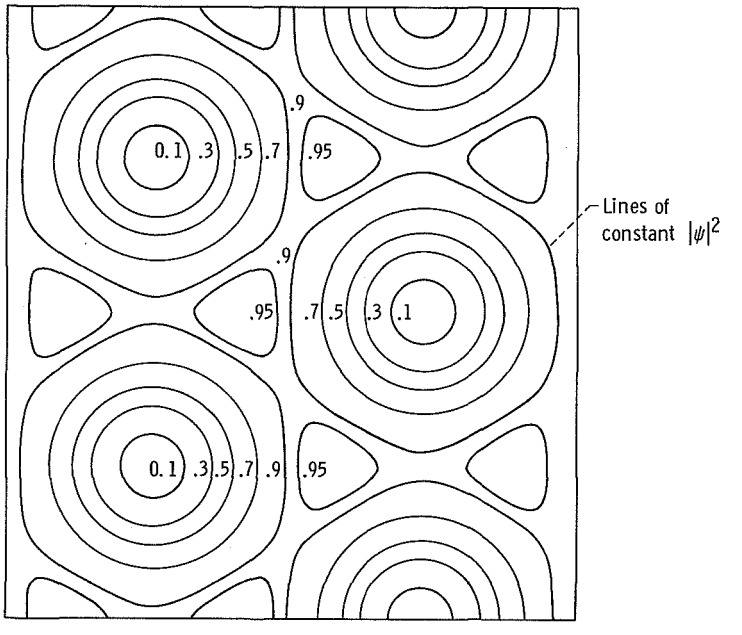

FIGURE 10.—Spatial variation of $|\psi|^2$ for triangular vortex lattice (ref. 40).

Gibbs Free Energy of Laminar Model and Vortex Model

The ultimate theoretical test is to compare the Gibbs free energy for both models and determine which state is energetically more favorable. In each case an expression for the Gibbs free energy is calculated and then minimized. The H_{c1} can be determined by analyzing the dependence of G_{min} on H. The minimum Gibbs free energy for the two models can then be compared using the H_{c1} values. The pedagogical development that follows is largely due to DeGennes (ref. 38).

The analysis is begun by calculating a general expression for the total free energy of a superconductor. The Helmholtz free energy is the sum of the kinetic energy and the magnetic energy:

$$\mathscr{F}_s = E_{kinetic} + E_{magnetic} + E_o \tag{45}$$

The magnetic energy is

$$E_{magnetic} = \int \frac{h^2}{8\pi}\, d\boldsymbol{r} \tag{46}$$

The kinetic energy is

$$E_{kinetic} = \int \left(\frac{1}{2}\, mv^2(r) n_s\right) d\boldsymbol{r} \tag{47}$$

The drift velocity $\boldsymbol{v}(r)$ is related to the current density by

$$n_s e \boldsymbol{v}(r) = \boldsymbol{j}(r) \tag{48}$$

The localized Maxwell equation is

$$\nabla \times \boldsymbol{h} = \frac{4\pi}{c}\, \boldsymbol{j}(r) \tag{49}$$

where $\boldsymbol{h}$ is the local value of the magnetic field intensity. Then solving equation (49) for $\boldsymbol{j}(r)$, substituting into equation (48), solving for $\boldsymbol{v}(r)$, and substituting into equation (47) yield

$$E_{kinetic} = \frac{1}{8\pi} \int d\boldsymbol{r} \lambda_L^2 |\nabla \times \boldsymbol{h}|^2 \tag{50}$$

Finally, substituting equations (46) and (50) into equation (45) results in

$$\mathscr{F}_s = E_o + \frac{1}{8\pi} \int (h^2 + \lambda_L^2 |\nabla \times \boldsymbol{h}|^2) d\boldsymbol{r} \tag{51}$$

In the following applications of equation (51), $E_o = 0$; that is, the normal state energy is taken as the zero of energy.

Free energy of laminar model.—As illustrated by the laminar structure shown in figure 11, the local field $\boldsymbol{h}$ is determined by the London equation (eq. (6)). In one dimension with the assumed model, the London equation is

$$\lambda^2 \frac{d^2h}{dx^2} = h \tag{52}$$

The solution in the superconducting region is

$$h = H_m \frac{\cosh\left(\frac{x}{\lambda}\right)}{\cosh P} \tag{53}$$

where $P = d/2\lambda$ and H_m is the field in the normal region. Then when equation (51) is modified for the laminar geometry, the Helmholtz free energy is

$$F_s = \frac{2}{d}\int_0^{d/2}\left[\frac{h^2 + \lambda^2\left(\frac{dh}{dx}\right)^2}{8\pi}\right]dx \tag{54}$$

Differentiating equation (53) with respect to x, squaring, and substituting the result and equation (53) into equation (54) yield

$$F_s = \frac{2\lambda}{8\pi d}\int_0^{d/2} d\left(\frac{x}{\lambda}\right)\left[\frac{H_m^2}{\cosh^2 P}\cosh^2\left(\frac{x}{\lambda}\right) + \frac{H_m^2}{\cosh^2 P}\sinh^2\left(\frac{x}{\lambda}\right)\right] \tag{55}$$

When equation (55) is integrated,

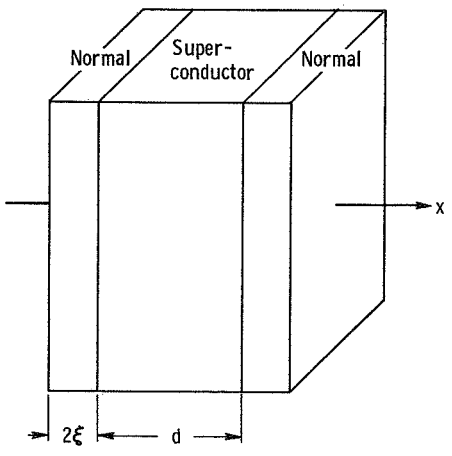

FIGURE 11.—Laminar model for mixed state.

$$F_s=\frac{1}{8\pi P}\frac{H_m^2}{\cosh^2 P}\frac{\sinh 2P}{2} \tag{56}$$

Using the multiple angle formula ($\sinh 2z=2\sinh z\cosh z$) gives

$$F_s=\frac{H_m^2}{8\pi}\frac{\tanh P}{P} \tag{57}$$

The free energy of the normal region is

$$F_n=\frac{H_c^2}{8\pi}\frac{2\xi}{d}=\frac{H_c^2}{8\pi}\frac{1}{Pk} \tag{58}$$

where $\kappa=\lambda/\xi$.

To convert the Helmholtz free energy to a Gibbs free energy, $-BH/4\pi$ must be added. Therefore, using the fact that B is the average of equation (53) in the superconducting region leads to

$$-\frac{BH}{\pi}=-\frac{Hh_{ave}}{4\pi}=-\frac{H}{4\pi}\left(\frac{2}{d}\int_0^{d/2}dxH_m\frac{\cosh\frac{x}{\lambda}}{\cosh P}\right)=-\frac{HH_m}{4\pi}\frac{\tanh P}{P} \tag{59}$$

Adding the three contributions to the Gibbs free energy of the lamina (eqs. (59), (58), and (57)) gives

$$G_{laminar}=\frac{H_m^2}{8\pi}\frac{\tanh P}{P}+\frac{H_c^2}{8\pi}\frac{1}{P\kappa}-\frac{HH_m}{4\pi}\frac{\tanh P}{P} \tag{60}$$

Minimizing $G_{laminar}$ with respect to H_m yields $H=H_m$. Then if d is $4\lambda_L$ or greater, $\tanh P\cong 1$ and

$$G_{laminar}=\frac{1}{8\pi P}\left(-H^2+\frac{H_c^2}{\kappa}\right) \tag{61}$$

Now keeping in mind that the equilibrium state of a system corresponds to a minimum in the Gibbs free energy, $G_{laminar}$ may be studied with respect to H. If $H_c<\sqrt{\kappa}$, then G is a minimum when P is infinite. Infinite P implies infinite d or a complete Meissner effect. If $H>H_c/\sqrt{\kappa}$ minimum G occurs for some finite P, which implies that it becomes energetically favorable for magnetic field to be inside the superconductor. The laminar state becomes favorable when

$$H=H_{c1}(laminar)=\frac{H_c}{\sqrt{\kappa}} \tag{62}$$

Free energy of vortex model.—The next step is to calculate H_{c1} for the vortex model. Once again, the Gibbs free energy is calculated and minimized to determine where the Meissner state breaks down. Near H_{c1} the interaction energy between flux lines can be ignored. The Gibbs free energy of a material is equal to the number of vortices per square meter (B/φ_o) multiplied by the Gibbs free energy per meter of a single vortex minus the magnetic field energy density:

$$G_{vortex}=B\left(\frac{Z}{\varphi_o}-\frac{H}{4\pi}\right) \tag{63}$$

where Z is the energy per unit length of a vortex. The energy Z can be calculated using equation (51):

$$l_f Z=\int_{(r>\xi)} d\boldsymbol{r}\,\frac{1}{8\pi}\,[h^2+\lambda^2(\nabla\times\boldsymbol{h})^2] \tag{64}$$

where l_f is the length of the flux line. This integration can be performed if the integral is first transformed to a surface integral (appendix C):

$$l_f Z=\frac{\lambda^2}{8\pi}\int d\boldsymbol{\sigma}\cdot[\boldsymbol{h}\times(\nabla\times\boldsymbol{h})] \tag{65}$$

When integration is performed on equation (65) for the surface of a cylinder of radius ξ, the integrand is constant by symmetry and l_f cancels out:

$$Z=\frac{\lambda^2}{8\pi}\,(2\pi\xi)h(\xi)|\nabla\times\boldsymbol{h}(\xi)| \tag{66}$$

The $h(\xi)$ and $|\nabla\times\boldsymbol{h}(\xi)|$ can be evaluated starting from the London equation

$$\boldsymbol{h}+\lambda^2(\nabla\times\nabla\times\boldsymbol{h})=\varphi_o\delta(r) \tag{67}$$

where

$$\delta(r)=\begin{cases}0 & r>\xi\\ 1 & r<\xi\end{cases}$$

If equation (67) is integrated over the area bounded by a circle C of radius r, which encloses the normal core, then

$$\int[\boldsymbol{h}+\lambda^2(\nabla\times\nabla\times\boldsymbol{h})]\cdot d\boldsymbol{\sigma}=\int\varphi_o\delta_2(\boldsymbol{r})\cdot d\boldsymbol{\sigma}=\varphi_0 \tag{68}$$

By Stokes' rule,

$$\int \boldsymbol{h} \cdot d\boldsymbol{\sigma} + \lambda^2 \oint |\nabla \times \boldsymbol{h}| \cdot d\boldsymbol{l} = \varphi_o \tag{69}$$

If $\lambda \gg r \gg \xi$, then $\int \boldsymbol{h} \cdot d\boldsymbol{\sigma} = 0$ because a negligible fraction r^2/λ^2 of the total flux is inside C. Then $\nabla \times \boldsymbol{h}$ may be assumed constant on C because of the cylindrical symmetry. Therefore,

$$|\nabla \times \boldsymbol{h}| = \frac{\varphi_o}{2\pi\lambda^2} \frac{1}{r} \tag{70}$$

The general solution of this equation is K_o, the modified Bessel function. If $\nabla \times \boldsymbol{h} = -d\boldsymbol{h}/dr$, integrating by separation of variables yields

$$h = \frac{\varphi_o}{2\pi\lambda^2} \ln \frac{\lambda}{r} \tag{71}$$

Now equation (66) can be evaluated at $r = \xi$ by substituting for h from equation (71) and for $|\nabla \times \boldsymbol{h}|$ from equation (70):

$$Z = \left(\frac{\varphi_o}{4\pi\lambda}\right)^2 \ln \left(\frac{\lambda}{\xi}\right) \tag{72}$$

And now, finally, the Gibbs free energy of the vortex G_{vortex} (eq. (63)) can be calculated. If $H < 4\pi Z/\varphi_o$, the minimum in G_{vortex} occurs at $B = 0$ (type I superconductor). If $H > 4\pi Z/\varphi_o$, then the minimum occurs when

$$\frac{dG_{vortex}}{dB} = \left(\frac{Z}{\varphi_o} - \frac{H}{4\pi}\right) = 0 \tag{73}$$

and magnetic field penetration occurs when

$$H = H_{c1} = \frac{4\pi Z}{\varphi_o} \tag{74}$$

Substituting equation (71) into equation (74) yields

$$H_{c1} = \frac{\varphi_o}{4\pi\lambda^2} \ln \left(\frac{\lambda}{\xi}\right) \tag{75}$$

Because the original goal of this section is to compare the free energies of the laminar model and the vortex model, equation (75) must be algebraically manipulated into a ratio of H_{c1}/H_c so that it can be compared with equation (62). This is done in appendix D and the result is

$$\frac{H_{c1}}{H_c} = \frac{\pi}{\sqrt{24}} \frac{\ln \kappa}{\kappa} \tag{76}$$

Comparison of Gibbs free energy of the two models.—Now the Gibbs free energy of the two models can be compared. In figure 12, H_{c1}/H_c is plotted as a function of κ for the functions derived in equations (62) and (76). The lower critical field H_{c1} is smaller for the vortex model than

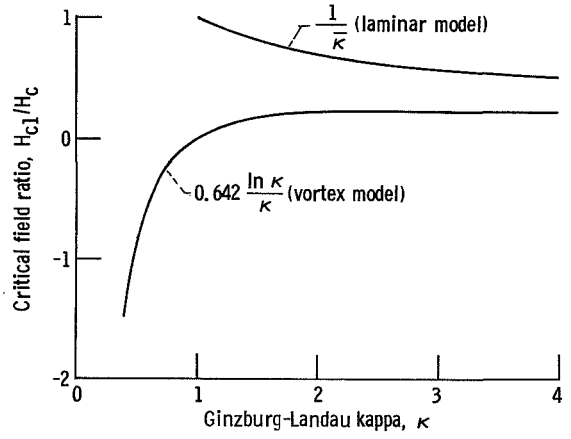

FIGURE 12.—Curves H_{c1}/H_c against κ for laminar model and vortex models are compared.

for the laminar model. When H is greater than H_{c1} (vortex) but less than H_{c1} (laminar), the Gibbs free energy of the vortex state is less than the free energy of the Meissner state. And the Gibbs free energy of the laminar state is equal to the free energy of the Meissner state. Therefore, when H is between H_{c1} (vortex) and H_{c1} (laminar), the Gibbs free energy of the vortex model is less than the free energy of the laminar model, and the vortex state is more favorable than the laminar state. DeGennes (ref. 42) has compared the states at higher magnetic fields and found that the vortex state is again more favorable. Goodman (ref. 43) has calculated the magnetization for both the vortex model and the laminar model. Figure 13 shows the comparison between these calculations and the magnetization measurements of Joiner and Blaugher (ref. 44) on $Mo_{0.85}Re_{0.15}$. Clearly, this result favors the vortex state. Subsequently, the vortex state has been substantiated by the NMR measurements of Pincus (ref. 45) and by the neutron diffraction experiments of Cribier (refs. 46 and 47).

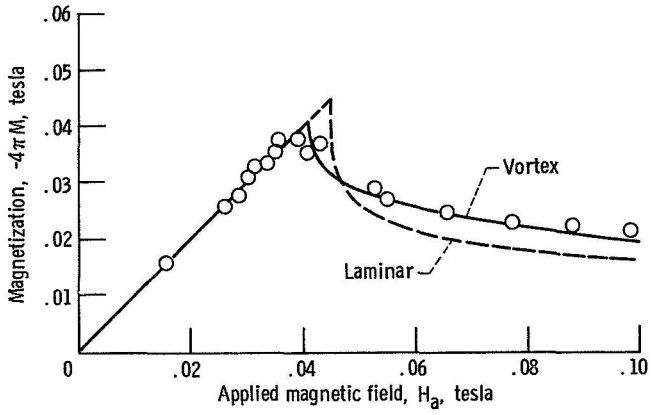

FIGURE 13.—Goodman's calculated magnetization curves for vortex and laminar states are compared with experimental data of Joiner and Blaugher (ref. 43.). Material, $Mo_{0.85}Re_{0.15}$; reduced temperature, $t = T/T_c = 0.522$.

The most convincing proof of the vortex state is the electron microscope pictures of U. Essmann and H. Trauble (ref. 48). They deposited iron on a lead-indium alloy in the mixed state. The flux lines in the alloy caused the iron to be deposited preferentially on the regions where the flux lines reside. An electron microscope picture of the result is shown in figure 14. A triangular lattice is formed by the flux lines in agreement

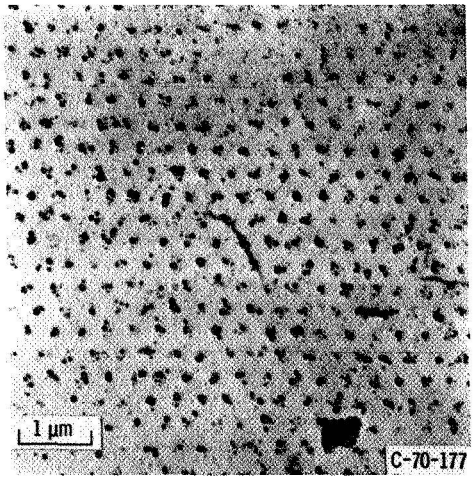

FIGURE 14.—Electron microscope picture of triangular lattice of flux lines on surface of lead-indium alloy (ref. 47). Distance between flux lines, ~ 1000 Å.

with the theoretical predictions. The flux quantum can be calculated by counting the dots and knowing the field of view and the magnetic field. The result is very close to 2×10^{-15} meter squared, tesla in agreement with predictions for the flux quantum.

This experiment implies that it is energetically more favorable to create additional vortices as the magnetic field penetrates rather than to increase the flux in each vortex. This is theoretically agreeable because in equation (72) doubling φ_0 results in a line energy of $4Z$ compared to a line energy of $2Z$ if another vortex is added. It is interesting to note that the flux lattice has many properties of crystal lattices, plastic distortions, line dislocations, stacking faults, point defects, and holes (ref. 48).

FLUX CREEP

In the INTRODUCTION mention was made of the anomalous electric, magnetic, and caloric behavior of alloys that was observed by Mendelssohn in 1934 and 1935. These experiments had the effect of focusing interest on alloy systems and lead to the discovery of the mixed state and type II superconductors. Some years later, Gorter (ref. 49) suggested that the Lorentz force resulting from electrical transport currents would cause regions of superconductivity to move and that this motion would result in energy dissipation. This concept along with the ideas of the mixed state and flux quantization set the stage for the discovery of flux creep and flux flow.

Tube Magnetization Experiments

Flux creep was first observed in tube magnetization experiments (ref. 50). The experimental setup, shown in figure 15, consists of a tubular sample with pickup coils inside and out. A probe for measuring magnetic field is in the bore of the tube. The magnetic field inside the tube H' is measured as an external magnetic field H is applied. Any flux that jumps into or out of the tube will be observed as transient induced voltages in the pickup coils. Abrupt changes in the flux in a material are referred to as flux jumps. Figure 15 also shows a plot of H' as a function of H for a 3Nb-Zr alloy at 4.2 K. Induced currents in the sample shield the bore from the external magnetic field H up to 0.31 tesla (curve A). Then the magnetic field begins to penetrate the bore and H' approaches asymtotically the value of H at very high field. When the external field is reduced (curve B), the magnetic field is trapped in the tube and the trapped field exceeds the applied field. The field H' becomes equal to zero at -0.31 tesla. When the same experiment was performed on a niobium powder sintered tube, the experimental data fell

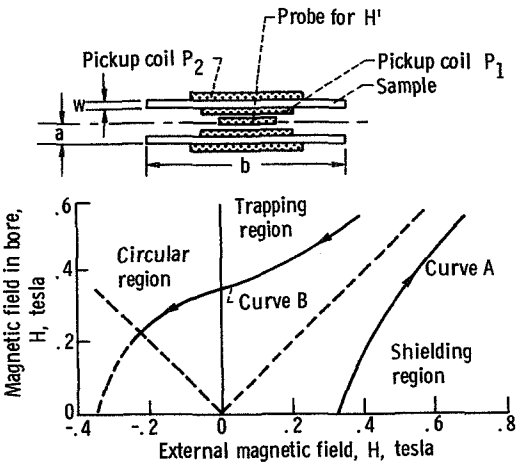

FIGURE 15.—Experimental setup for tube magnetization experiments is shown and magnetic field in the bore H of the tube is plotted against the field H outside the tube (ref. 49). Tube material, 3Nb-Zr; tube temperature, 4.2 K.

on a straight line when the magnetic fields H and H' were related by

$$\frac{4\pi w\alpha_c}{|\mathcal{M}|}=B_o+H^* \tag{77}$$

where w is the tube thickness, $|\mathcal{M}|=H-H'$, and $H^*=\frac{1}{2}(H'+H)$. The B_o and α_c are constants. Kim, Hempstead, and Strnad were able to show that $|\mathcal{M}|$ is proportional to the current in the sample, which leads to the critical state equation

$$\alpha_c = J(B + B_o) \tag{78}$$

If $J(B + B_o) > \alpha_c$, then magnetic flux enters the tube.

Kim, Hempstead, and Strnad also made two other very interesting observations. If H is held constant, they found that $|\mathcal{M}|$ decays logarithmically with time. Apparently the shielding currents decay in time, the magnetic field enters the sample, moves through it, and into the bore of the tube. They also noted that when the external field was being increased the flux entering the sample induced observable voltages in pickup coil P_1 but not in P_2 (see fig. 15). When the magnetic field was being decreased, the flux leaving the sample induced observable voltages in pickup coil P_2, but not in P_1. The smallest signals measured were estimated to correspond to 20 to 50 flux quanta. One possible explanation

for this observation is that flux enters the sample in unmeasurably small increments, perhaps individual flux quanta, but leaves the sample in increments of 20 to 50 quanta.

Flux Motion Resistivity

The observed decay of superconducting currents implies the existence of a resistance in the tube. The resistivity ρ of the tube can be derived by using a long solenoid approximation to get the current and by approximating the tube with an equivalent LR circuit. The result is

$$\rho = \frac{2\pi a w}{H' - H} \frac{dH'}{dt} \tag{79}$$

The existence of a mixed state resistance suggests that if a transport current is applied to a material in the mixed state, voltages should be observed. Kim, Hempstead, and Strnad (ref. 50) have in fact observed such voltages in NbZr. Figure 16 shows that these experimental data are

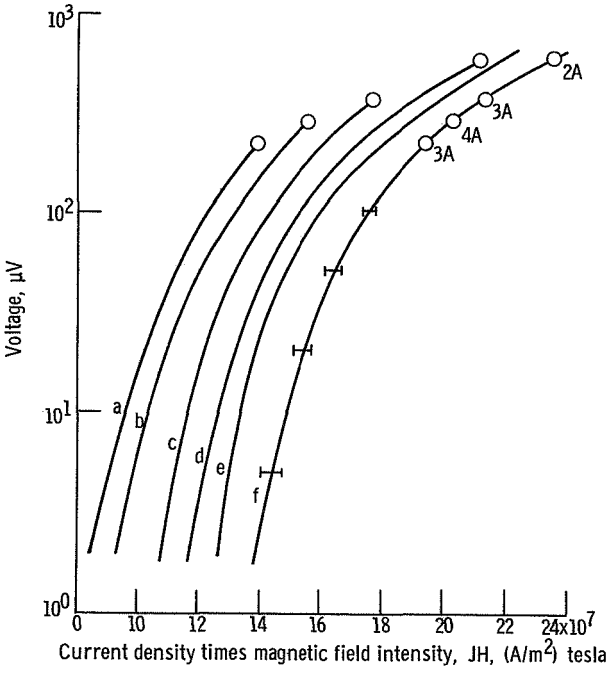

FIGURE 16.—Voltage V is plotted as function of JH for curves corresponding to given current densities. Curve f is a plot of V against $J(H+B_a)$ for all other curves (ref. 49). Alloy, 3Nb-Zr wire; wire temperature, 4.2 K.

fitted by an equation of the form

$$\ln V = J(H + B_o) \tag{80}$$

Anderson and Kim (ref. 51) suggested a possible mechanism for the apparent movement of magnetic flux in type II superconductors. Anderson and Kim called the flux movement "flux creep" and postulated the following mechanism (see fig. 17). Flux quanta penetrate the sample individually when the sample goes into the mixed state (fig. 17(a)). But once inside, the flux quanta form into bundles (fig. 17(b)) which are approximately the penetration depth in diameter. Inside each bundle the Abrikosov triangular flux lattice structure is postulated to exist (fig. 14). The postulate is consistent with the flux jumps observed in the pickup coils. They further postulate that the free energy of a superconductor varies spatially due to inhomogeneities, strains, dislocations, and other physical defects. These free energy variations provide pinning sites for

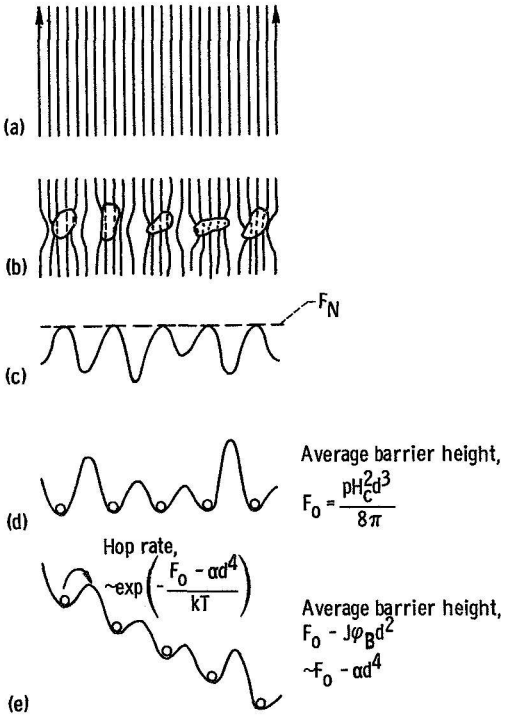

FIGURE 17.—Sketch of Kim-Anderson flux bundles and some other properties of flux creep mechanism (ref. 49).

the flux bundles. The strained regions have larger free energies than the unstrained regions (fig. 17(c)). These maxima in the free energy of the material represent minima for the free energy of the flux lines (fig. 17(d)) because less energy is required to establish a normal core. The pinned flux lines therefore are surrounded by a free energy barrier. Anderson and Kim estimate the maximum free energy barrier to be

$$\Delta G_{max} = (G_n - G_s) d^3 = \left(\frac{H_c^2}{8\pi}\right) \xi_o^3 \tag{81}$$

where the size of the inhomogeneity d is assumed to be about equal to ξ_o. They further propose that a Lorentz type force acts on the flux bundles. This concept was suggested by the empirical critical state equation (eq. (78)). Flux creep occurs when the flux bundle is momentarily thermally excited to a free energy greater than the pinning energy. The Lorentz force then causes the bundle to move until it is caught by a pinning site (fig. 17(e)). Apparently, the thermal energy must then be lost to other flux bundles or to the crystal lattice; otherwise, the bundle would not become repinned.

Anderson and Kim have also postulated that the rate R at which flux lines hop from one pinning site to the next is proportional to the negative exponential of the total barrier free energy. The total free energy is composed of two parts—the fraction p of equation (81) that is effective in pinning and the free energy associated with the Lorentz force. The Lorentz force per unit length of a flux line is

$$f_L = \frac{J\varphi_o}{c} \tag{82}$$

where c is the speed of light and $\varphi_o = hc/2e$. The force on a whole bundle is

$$f_L = \frac{J\varphi_B l'}{c} = \frac{JH\lambda^2 l'}{c} = \frac{J\varphi_o n_B l'}{c} \tag{83}$$

where φ_B is the flux in a bundle, n_B the number of flux lines in a bundle, and l' the effective length of a flux line (distance between pinning sites). The associated free energy F_L as a function of position x is

$$F_L = \frac{JH\lambda^2 l' x}{c} \tag{84}$$

This free energy of the flux bundle reduces the effective barrier free

energy that is pinning the bundle. The total effective barrier free energy F_T is then

$$F_T=\left(p\,\frac{H_c^2}{8\pi}\,\xi_o^3\right)-\left(\frac{JH\lambda^2 l\xi_o}{c}\right) \tag{85}$$

In this equation p is an adjustable parameter that ranges between zero and one to allow adjustment for the fraction of the maximum pinning energy that is effective. Next Anderson and Kim use the postulate that the number of flux bundles with a certain free energy decreases exponentially with the free energy. This implies that the thermal activation of flux lines in the bundle over a free energy barrier is governed by a hop rate R of the form

$$R=\omega_o e^{-F_T/kT} \tag{86}$$

In this equation ω_o, which is the vibrational frequency of the bundle, is estimated to be between 10^5 and 10^{10} hertz. The flux bundles move in the direction of the gradient of magnetic pressure $\boldsymbol{\alpha}$, which may be defined as

$$\boldsymbol{\alpha}=\nabla\left(\frac{H^2}{8\pi}\right)=\frac{\boldsymbol{J}\times\boldsymbol{H}}{c} \tag{87}$$

Then if the pinned flux bundles are viewed as a supply of flux lines, the flux entering and leaving a small volume obeys the diffusion equation

$$\frac{d\boldsymbol{B}}{dt}=-\nabla\left(\frac{\varphi_o R}{\lambda}\right) \tag{88}$$

These equations ((85), (86), (87), and (88)) can be combined to study flux motion in the tubular geometry of the tube magnetization experiments. In one dimension the diffusion equation becomes

$$\frac{\partial H}{\partial t}=-\frac{\partial}{\partial x}\left(\frac{\varphi_o R}{\lambda}\right) \tag{89}$$

and the magnetic pressure is

$$\alpha=-\frac{H}{4\pi}\frac{\partial H}{\partial x} \tag{90}$$

Then taking the time derivative of α and substituting for $\partial H/\partial t$ from equation (89) yield

$$\frac{\partial \alpha}{\partial t} = \frac{1}{4\pi} \frac{\varphi_o}{\lambda} \frac{\partial H}{\partial x} \frac{\partial R}{\partial x} + \frac{H}{4\pi} \frac{\varphi_o}{\lambda} \frac{\partial^2 R}{\partial x^2} \tag{91}$$

If equation (86) for R is written in terms of α (by substituting eq. (87) into eq. (85) and then substituting the result into eq. (86)) and the result is substituted into equation (91), then

$$\frac{\partial \alpha}{\partial t} = K_o \frac{\partial H}{\partial x} \frac{\partial e^{\alpha/\alpha_1}}{\partial x} + K_o H \frac{\partial^2 e^{\alpha/\alpha_1}}{\partial x^2} \tag{92}$$

where

$$\alpha_1 = \frac{kT}{\lambda^2 l \xi_o}$$

$$K_o = \left(\frac{\varphi_o \omega_o}{4\pi\lambda}\right) e^{-F_o/kT}$$

If the magnetic field is assumed to be uniform, then $\partial H/\partial x = 0$ and the first term on the right side of equation (92) vanishes. The remaining differential equation has a particular solution of the form

$$\alpha = \alpha_1 \left(\ln \frac{-\alpha_1 x^2 + bx + c}{2K_o} - \ln t \right) \tag{93}$$

This result agrees with the logarithmic time decay of the magnetic field trapped inside tubes of Kim's tube magnetization experiments (ref. 52). Furthermore, if equation (86) is solved for α (as described in the derivative of eq. (92)) and it is assumed that there is some critical R_c which corresponds to the lowest hop rate that can be observed experimentally, then an equation very much like equation (78) can be derived.

Kim and Anderson also derived the experimental result equation (80) and the power dissipation from Faraday's law:

$$\nabla \times \boldsymbol{E} = -\frac{1}{c} \frac{\partial \boldsymbol{B}}{\partial t} \tag{94}$$

In one dimension,

$$\frac{dE_y}{dx} = -\frac{1}{c} \frac{\partial B_z}{\partial t} = \frac{\varphi_o}{c\lambda} \frac{\partial R}{\partial x} = \frac{\varphi_o \omega_o}{\lambda c} \frac{\partial}{\partial x} \left(e^{-F_o/kT} e^{\alpha/\alpha_1}\right) \tag{95}$$

where $F_o = p(H_c^2/8\pi)\xi_0^3$. Integrating with respect to x gives

$$E_y = \frac{\varphi_o \omega_o}{\lambda c} e^{\left(-\frac{F_o}{kT} + \frac{\alpha}{\alpha_1}\right)} \tag{96}$$

The power dissipated P is then

$$P = E_y J_y = \frac{J \varphi_o \omega_o}{\lambda c} e^{\left(\frac{\alpha}{\alpha_1} - \frac{F_o}{kT}\right)} \tag{97}$$

The existence of power dissipation is consistent with the severe thermal instabilities observed in superconductors that carry high current density in large magnetic fields.

Kim, Hempstead, and Strnad (ref. 49) have found that in the limit of large values of α the exponential hop rate law (eq. (86)) is no longer applicable. Instead, R is proportional to α. This might be expected because for large α, $F_o - (\alpha/\alpha_1)kT$ becomes comparable to kT. This new regime is called the flux flow state.

FLUX FLOW

Early Flux Flow Experiments

Kim, Hempstead, and Strnad first observed the flux flow state as a deviation from the flux creep results (ref. 49). In figure 16 the composite curve f would be a straight line if flux creep were the only cause of the voltage. But at larger values of α, the curve bends over indicating that a new mechanism is contributing to the voltage. They measured the voltage-current—magnetic-field characteristics of several different materials. Figure 18 shows some examples of their results for NbTa and PbIn. These measurements were made with the magnetic field perpen-

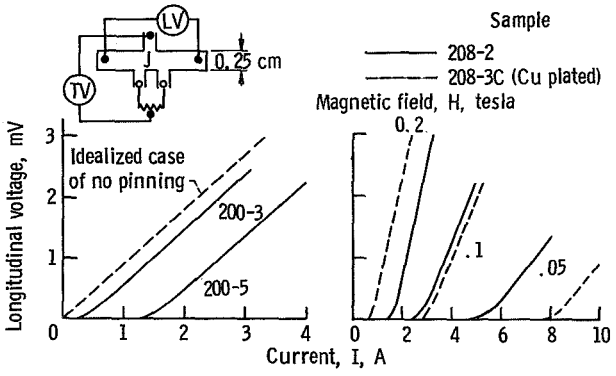

(a) Two samples of $Nb_{0.5}Ta_{0.5}$ with different amounts of pinning. Temperature, 3 K; magnetic field, 0.2 tesla.

(b) Comparison for three different magnetic fields and also for plated and unplated samples of $Pb_{0.83}In_{0.17}$. Temperature, 2 K.

FIGURE 18.—Flux flow voltage is shown as function of current (ref. 53).

dicular to both the surface of the samples and the applied current. Voltage appears when the current is greater than some magnetic-field-dependent onset values. The voltage is directly proportional to the current above the onset current. The voltage is also observed to be an increasing function of the magnetic field (fig. 18(b)). At temperatures sufficiently below the critical temperature T_c, the ratio of the flux flow resistivity ρ_f to the normal resistivity ρ_n obeys the simple relation

$$\frac{\rho_f}{\rho_n}=\frac{H}{H_{c2}} \tag{98}$$

This relation is very suggestive of a law of corresponding states. A resistivity like ρ_f would be observed if the current flowed uniformly through the superconducting regions and the normal cores of the flux vortices.

At first thought it seems unlikely that the current could flow uniformly through both the superconducting regions and the normal regions. The superconducting regions should simply electrically short the normal regions. If, however, the flux flow state is similar to the flux creep state, then the flux lines move under a Lorentz force. Also, the motion might generate electric fields that drive current through the normal cores. This would result in a resistivity that is proportional to the number of flux lines inside the superconductor. The model just described was first proposed by Kim, Hempstead, and Strnad (ref. 53).

The flux flow voltage can be expressed as a function of J and H. Figure 19 shows a type II superconductor with the magnetic field perpendicular to the current and to the surface of the superconductor. The vortices are

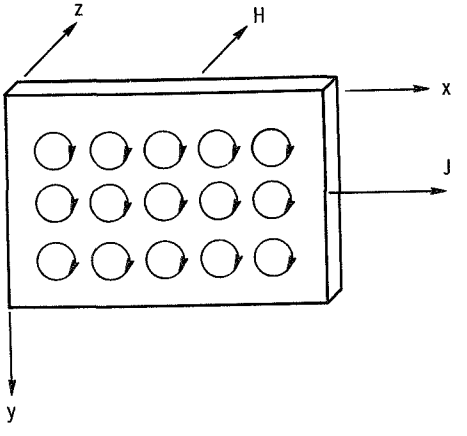

FIGURE 19.—Flux flow state.

indicated by simple current loops. The magnetic flux density equals the density of flux lines multiplied by the flux quantum:

$$\boldsymbol{B}=n\varphi_0\simeq\boldsymbol{H} \tag{99}$$

The magnetic intensity and the current density are related by Ampere's law:

$$\nabla\times\boldsymbol{H}=\hat{\imath}\,\frac{\partial H}{\partial y}=\hat{\imath}\varphi_0\,\frac{\partial n}{\partial y}=\frac{4\pi}{c}\,\boldsymbol{J} \tag{100}$$

The magnetic pressure is

$$\frac{\partial}{\partial y}\left(\frac{H^2}{8\pi}\right)=\frac{H}{4\pi}\frac{\partial H}{\partial y}=\frac{H}{4\pi}\left(\frac{4\pi}{c}J\right)=\frac{HJ}{c}=\frac{n\varphi_0}{c}J \tag{101}$$

And if the magnetic pressure is distributed evenly over all the flux lines, the Lorentz force on each flux line per unit length is

$$f_L=\frac{J\varphi_0}{c} \tag{102}$$

When the Lorentz force is greater than the pinning force, the flux line moves. It is further postulated that the flux lines experience a viscous drag force. The flux line accelerates until the viscous drag force balances the Lorentz force:

$$f_L=\eta v_L \tag{103}$$

where η is a viscosity parameter and v_L is the terminal velocity of the flux line. The power P dissipated per unit volume by the viscous flow is

$$P=nf_Lv_L=\frac{n}{\eta}\,\frac{J^2\varphi_0^2}{c^2} \tag{104}$$

Therefore, it is possible to derive the voltage per unit length V from equation (104) for $P=VJ$ and $H=n\varphi_0$:

$$V=\frac{\varphi_0}{\eta c^2}JH \tag{105}$$

The linear dependence of V on J is in agreement with the experimental results shown earlier (fig. 18). The magnetic field and the temperature dependence is shown by figure 20. The flux flow resistivity $\rho_f=V/J$ is directly proportional to the magnetic field when $T\ll T_c$.

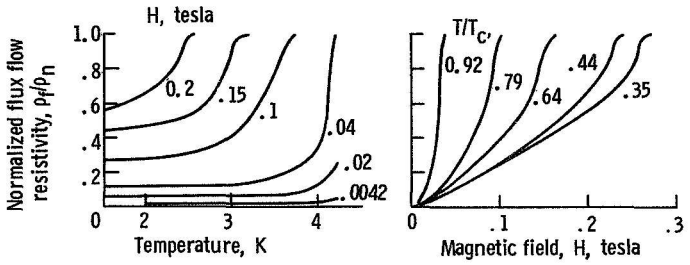

FIGURE 20.—Normalized flux flow resistivity plotted against magnetic field at several reduced temperatures for $Nb_{0.1}$ $Ta_{0.9}$. Resistivity also shown plotted against temperature at several values of magnetic field. Flux flow resistivty is normalized to normal state resistivity (ref. 54).

Other Flux Motion Experiments

There are other experiments which support the concept of flux motion and the flux flow voltage. Pearl (ref. 55) proposed to test the concept of a potential difference resulting from flux motion. He proposed to produce a continuous motion of flux lines by some external means and to look for a voltage. Later (ref. 56) he built such an apparatus (fig. 21). Magnetic field lines extending from the screw to the iron shell could be moved through the superconductor by rotating the screw. No transport current was passed through the sample, and yet voltages were observed across the sample that were roughly proportional to the rate of rotation.

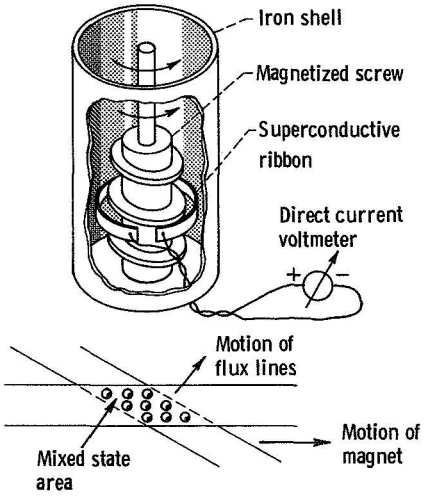

FIGURE 21.—Apparatus used by Pearl to investigate flux flow voltage (ref. 56).

Hans Meissner (ref. 57) performed another experiment which tends to confirm the concept of the motion of flux lines under a transport current induced Lorentz force. Meissner introduced a flux bundle on one side of a tin (Sn) film and observed it some time later with a pickup coil on the other side of the film. The flux flow velocity is determined by measuring the transit time and the film width. Meissner has observed flux flow velocities between 3×10^2 and 50×10^2 meters per second with current densities up to 10^9 amperes per square meter.

Another experiment on thin films by Giaever (refs. 58 and 59) contributed results which were consistent with the flux flow model. Giaever investigated the properties of two parallel thin films, 1000 Å thickness, in a perpendicular magnetic field. When he passed current through the primary film, he observed voltages across both the films. Figure 22 shows the model he proposed to explain these results. Both films are

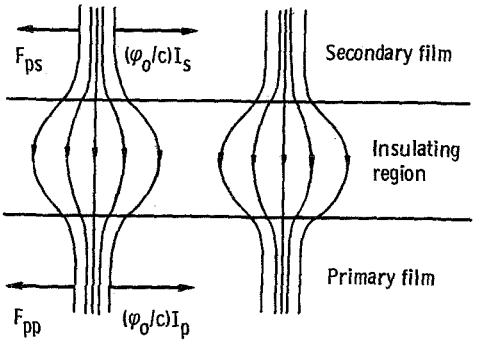

FIGURE 22.—Flux sharing model proposed by Giaever to explain his experimental results (ref. 59).

assumed to share the same flux bundles. When the transport currents in the primary film are sufficient to overcome pinning, the flux moves in both films. Therefore flux flow voltages are observed in both films. Some of Giaever's results are shown in figure 23, which shows the voltage in the primary film when the current is applied to both the primary and the secondary films. The family of curves shows that the current in the secondary apparently exerts a force on the flux line which can either add to or subtract from the force exerted by the current in the primary.

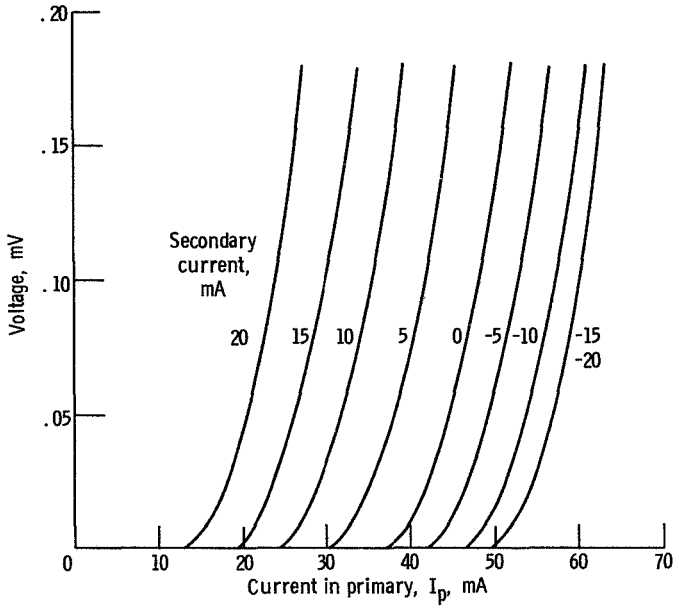

FIGURE 23.—Voltage across primary film plotted against primary current for various currents in secondary film (ref. 59). Temperature, $T = 3.65$ K.

Theoretical Basis for the Flux Flow Voltage

The exact nature of the source of the flux flow voltage has caused considerable controversy. The fact that ρ_f is proportional to H, or the number of normal cores (eq. (98)), suggests that the voltage is caused by transport current flowing through the normal cores of moving flux lines. However, Hempstead and Kim (ref. 60) suggested that the flux flow voltage was an induction voltage. Several authors (refs. 61 and 62) have argued that in the standard flux flow experiments the flux lines move across the sample but that $\partial \boldsymbol{B}/\partial t = 0$ and therefore no induction voltage can exist. Other authors (refs. 63 and 64) argued that $\partial \boldsymbol{B}/\partial t = 0$ means only that $\nabla \times \boldsymbol{E} = 0$ and not that $\boldsymbol{E} = 0$.

Goodman (ref. 65) has successfully derived the flux flow voltage from a local version of the second Ginzburg-Landau equation. Ignoring the first term on the right side of equation (22), the starting equation is

$$\nabla^2 a = -\frac{4\pi \boldsymbol{j}}{c} = \frac{16\pi e^2 \psi_0^2}{mc^2}\left(\boldsymbol{a} - \frac{\hbar}{2e}\nabla\theta\right) \tag{106}$$

where a is the local value of the magnetic vector potential, j is the local current density, $\psi = \psi_0 e^{i\theta}$, and $\nabla\theta$ is defined by the relation

$$\oint d\boldsymbol{l} \cdot \nabla\theta = 2\pi n_B \tag{107}$$

where n_B is the number of flux quanta per bundle. He also defines the average density of vortex lines $\boldsymbol{N}$ and an incremental area $d\boldsymbol{S}$. It is assumed that $d\boldsymbol{S}$ is much larger than the distance between flux lines. Then taking a line integral of the Ginzburg-Landau equation yields

$$-\frac{4\pi}{c}\oint_{dS} \boldsymbol{j} \cdot d\boldsymbol{l} = \frac{16\pi e^2\psi_o^2}{mc^2}\left(\oint_{dS} \boldsymbol{a} \cdot d\boldsymbol{l} - \oint_{dS} \frac{\hbar}{2e}\nabla\theta \cdot d\boldsymbol{l}\right) \tag{108}$$

Converting equation (108) to surface integrals using Stokes' theorem gives

$$-\frac{4\pi}{c}\int_{dS} (\nabla \times \boldsymbol{j}) \cdot d\boldsymbol{S} = \frac{16\pi e^2\psi_o^2}{mc^2}\left[\int_{dS} (\nabla \times \boldsymbol{a}) \cdot d\boldsymbol{S} - \boldsymbol{N}\varphi_o\right] \tag{109}$$

Recalling that $\psi_o^2 = n_S$ and $\lambda_L^2 = mc^2/4\pi n_S e^2$ and substituting yield

$$\boldsymbol{H} + \frac{4\pi}{c}\lambda_L^2 (\nabla \times \boldsymbol{J}) = \boldsymbol{N}\varphi_o \tag{110}$$

where $\boldsymbol{H}$ and $\boldsymbol{J}$ are the mean field and current density. Equation (110) can be written in either of the following forms using Ampere's law ($\nabla \times \boldsymbol{H} = (4\pi/c)\boldsymbol{J}$):

$$\boldsymbol{H} - \lambda_L^2\nabla^2\boldsymbol{H} = \boldsymbol{N}\varphi_o \tag{111a}$$

or

$$\boldsymbol{J} - \lambda_L^2\nabla^2\boldsymbol{J} = \frac{\varphi_o}{4\pi}(\nabla \times \boldsymbol{N}) \tag{111b}$$

Thus, if $\boldsymbol{N}$ is known, $\boldsymbol{J}$ and $\boldsymbol{H}$ are specified. Next Goodman assumes a vortex line continuity equation:

$$\nabla \times (\boldsymbol{v}_L \times \boldsymbol{N}) = \frac{\partial \boldsymbol{N}}{\partial t} \tag{112}$$

Then taking the time derivative of equation (110) gives

$$\frac{\partial \boldsymbol{H}}{\partial t} + 4\pi\lambda_L^2\left[\nabla \times \left(\frac{\partial \boldsymbol{J}}{\partial t}\right)\right] = \varphi_o\frac{\partial \boldsymbol{N}}{\partial t} \tag{113}$$

Substituting equation (112) and Faraday's law of induction ($\nabla \times \boldsymbol{E} = -(1/c)(\partial \boldsymbol{H}/\partial t)$) into equation (113) yields

$$-\nabla \times \boldsymbol{E} + \frac{4\pi}{c}\lambda_L^2\left[\nabla \times \left(\frac{\partial \boldsymbol{J}}{\partial t}\right)\right] = \frac{\varphi_o}{c}\left[\nabla \times (\boldsymbol{v}_L \times \boldsymbol{N})\right] \tag{114}$$

Equation (115) is obtained by eliminating the curl on both sides of the equation and setting $\partial \boldsymbol{J}/\partial t = 0$:

$$\boldsymbol{E} = \frac{\varphi_o}{c}\boldsymbol{N} \times \boldsymbol{v}_L) \tag{115}$$

Goodman has ignored any possible constant terms and gradient terms in equation (115). Equation (115) is identical to the electric field that is measured by a stationary observer in a coordinate system moving with a changing magnetic field (ref. 66).

THEORIES OF THE MOTION OF VORTICES IN SUPERCONDUCTORS

Before going into the two major theoretical models that have been proposed for flux flow, it is possible to gain some insight into the problem by a simple analysis of the change in momentum resulting from the motion of a single vortex. Figure 24 is a sketch of a normal core (radius r) moving with velocity $\boldsymbol{v}_L$. Outside the core the superconducting electrons of the vortex are assumed to have momentum:

$$p_\theta = -\frac{\hbar}{2r} \tag{116}$$

When the vortex moves as shown, the superconducting electrons on the front boundary of the core are converted to stationary normal electrons. The resulting momentum loss in the boundary layer is approximated by

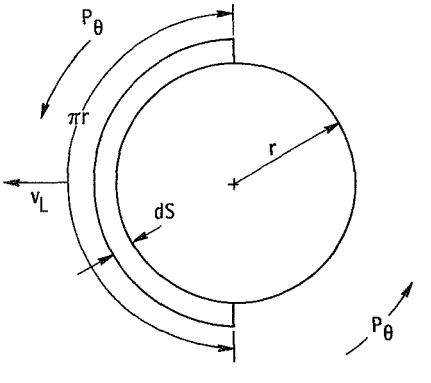

FIGURE 24.—Normal core (radius r) moving with velocity v_L.

$$\frac{d\boldsymbol{p}}{dt}=\frac{(\text{Number of electrons})(\text{Momentum change})}{\text{Time interval}}=\frac{(\pi r n_s ds)p_\theta}{dt} \tag{117}$$

Setting $\boldsymbol{v}_L=ds/dt$ and substituting equation (116) into equation (117) gives

$$\frac{d\boldsymbol{p}}{dt}=-\frac{1}{2}\pi n_s\hbar\boldsymbol{v}_L \tag{118}$$

Finally, substituting for $\hbar$ from $\varphi_o=hc/2e$ yields

$$\frac{d\boldsymbol{p}}{dt}=-\frac{1}{2}\frac{n_s e}{c}\boldsymbol{v}_L\varphi_o \tag{119}$$

Because an equal amount of momentum must be added on the right side of the vortex, the resulting momentum lost must be twice equation (119). The theories of Bardeen-Stephen and Nozieres-Vinen (which follow) postulate mechanisms for this momentum loss. The rate of change of momentum corresponds to a Magnus type force (ref. 67), which acts on the vortex and is perpendicular to its direction of motion.

Bardeen-Stephen Theory

Two theoretical models have been proposed which attempt to explain the phenomena of vortex motion in type II superconductors. The theory of Bardeen and Stephen (ref. 68) finds that, if the transport current causes a force on the flux line, the resulting motion generates an electric field that drives the current through the normal core of the vortex.

Bardeen and Stephen assume that the Lorentz force $\boldsymbol{J}\varphi_o/c$ is the driving force on the flux lines. They assume that the most important scattering process is electron-lattice scattering rather than electron-electron scattering. An isolated vortex is considered; the temperature is near $T=0$ K and the mean free path is assumed to be greater than the coherence distance. Bardeen and Stephen assume that the flux line contains a normal core. This means that the energy gap Δ is equal to zero inside the core. Outside the core there is assumed to be a transition region where the energy gap increases from zero to its equilibrium value. They further assumed that the transport current density and the normal current density generated by the motion are small compared with the supercurrent flow just outside the core. Then they studied the current distribution in the transition region starting with the equation of motion from the local London theory:

$$\frac{d\boldsymbol{v}_s}{dt}=-\nabla\mu_o+\frac{e}{m}\left[\boldsymbol{E}+\frac{1}{c}(\boldsymbol{v}_s\times\boldsymbol{H})\right] \tag{120}$$

where μ_o is the chemical potential per unit mass with zero current and field. They succeed in deriving expressions for the components of the velocity of the normal and superconducting electrons. Combining these equations with calculations of the power dissipation inside and outside the core, they obtain several interesting results. First, the velocity of electrons inside the core is equal to the velocity of the electrons in the transport current. If the core radius r_o is assumed to be related to H_{c2} by

$$\frac{\varphi_o}{2\pi r_o^2}=H_{c2}-\frac{H}{2} \tag{121}$$

the law of corresponding states (eq. (98)) can be derived. They also conclude that the Hall angle θ_H is equal to the Hall angle of the normal material at the magnetic field in the normal core; therefore,

$$\tan\theta_H=\left(\frac{e\tau}{mc}\right)H \tag{122}$$

where τ is the normal electron relaxation time. This same result was obtained earlier by Miller (ref. 69) using a two fluid model.

Nozieres-Vinen Model

The other theoretical model was proposed by Nozieres and Vinen (ref. 70). Nozieres and Vinen proposed that the motion of flux lines is analogous to the motion of vortices in liquid helium. The vortex of superconducting electrons is subject to a Magnus force, which is perpendicular to the direction of vortex motion. DeGennes and Matricon (ref. 71) had proposed a similar concept earlier. They considered the force on a flux line with an applied transport current. In a reference frame moving at a constant velocity v_L, superfluid electrons represent the current

$$j=n_s(-e)(-v_L) \tag{123}$$

Therefore, the force per unit length on the flux line is

$$f_L=\frac{j\varphi_o}{c}=-n_se\left(\frac{v_L}{c}\right)\varphi_o \tag{124}$$

The Nozieres and Vinen model incorporates the following assumptions. The penetration depth is much greater than the coherence length. The material is homogeneous, with the mean free path much greater than the coherence length. The temperature is near 0 K so that no normal excitations exist outside the core. The velocity distribution of the other vortices

is assumed to be constant over the core of the vortex, with a sharp boundary assumed for the core. Far outside the core the London equation is assumed to be obeyed. The entire development is carried out in the crystal lattice frame of reference to avoid problems with the effect of the positive background. Then, using the London and Maxwell equations together with Euler's equation for a nonviscous charged fluid (ref. 33),

$$\frac{d(\boldsymbol{v}_s-\boldsymbol{v}_L)}{dt}=\frac{\partial \boldsymbol{v}_s}{\partial t}+(\boldsymbol{v}_s\cdot\nabla)\boldsymbol{v}_s=\frac{\partial \boldsymbol{v}_s}{\partial t}+\frac{1}{2}\nabla(\boldsymbol{v}_s-\boldsymbol{v}_L)^2 - (\boldsymbol{v}_s-\boldsymbol{v}_L)\times(\nabla\times\boldsymbol{v}_s) \qquad (125)$$

where $\boldsymbol{v}_s$ is the total superfluid velocity and $\boldsymbol{v}_L$ is the velocity of the flux line, they derive Bernoulli's theorem for the charged fluid:

$$\mu+eV+\frac{m}{2}(\boldsymbol{v}_s-\boldsymbol{v}_L)^2=\text{Constant} \qquad (126)$$

Next they derived the force on a line by considering the flow pattern in the vortex frame. To do this they constructed a cylinder of radius $r\gg\xi$ which was concentric to the flux line. Then, summing the electromagnetic forces, the fluid pressure, and the forces caused by the net momentum flowing through the surface of the cylinder yielded the total force as

$$\boldsymbol{F}=\frac{Ne}{c}(\boldsymbol{v}_{s1}-\boldsymbol{v}_L)\varphi_o \qquad (127)$$

where $\boldsymbol{v}_{s1}$ is the local superfluid velocity in which the line is moving. This force per unit length is the Magnus force.

The concept of using the equations of fluid mechanics to describe superconductivity is not new, it was first proposed in 1933 (ref. 17). London derives equations (125) and (126) in a discussion of these earlier attempts (ref. 33).

Then when the vortex core is approximated by a normal cylinder with radius a, the electrons in the core are assumed to have a uniform drift velocity $\boldsymbol{v}_{nc}$. At the boundary between the core and the remainder of the vortex there is a discontinuity in the superconducting wave function. Following Bardeen and Stephens, Nozieres and Vinen assume $\boldsymbol{v}_{nc}=\boldsymbol{v}_{s1}$. They also assume that the Magnus force is divided evenly between the region outside the core and bulk of the core. The surface part of the total force would come from an electrostatic contact potential at the interface. They then assume that no contact potential exists and set the remaining half of the Magnus force equal to the rate that momentum is being lost in the core. This gives the equation of motion of the normal

cores:

$$\frac{1}{2}\frac{Ne}{c}(\boldsymbol{v}_{s1}-\boldsymbol{v}_L)\times\boldsymbol{\varphi}-Nm\frac{\boldsymbol{v}_{s1}}{\tau}\pi a^2=0 \tag{128}$$

This equation may be compared to the Bardeen-Stephen result if the relation between core radius and field is

$$\frac{\varphi}{2\pi a^2}=H_{c2} \tag{129}$$

When this is substituted into equation (128) the resulting equation is then solved for the resistivity and yields the law of corresponding states (eq. (98)). The Hall angle that results from the Nozieres-Vinen analysis is independent of magnetic field:

$$\tan\theta_H=\frac{eH_{c2}}{mc}\tau \tag{130}$$

Comparison Between Theoretical Predictions and Experimental Results

An obvious experimental test of these two theories is to measure the Hall angle and determine whether or not it has a magnetic field dependence. Figure 25 shows the Hall angle predictions of the two models. The

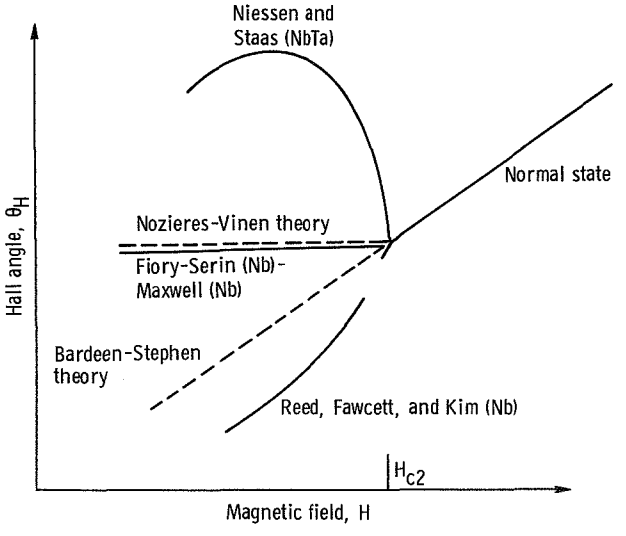

FIGURE 25.—Theoretical predictions of Bardeen-Stephen and Nozieres-Vinen are compared with experimental results.

presently available experimental data are also included in the figure. The results of Niessen and Staas (ref. 72) on dirty (mean free path $\ll \xi_o$) NbTa does not agree with either theory. Very recently a similar experimental result was obtained by Hake (ref. 73) on TiMo. Hake also finds the Hall angle in the mixed state to be greater than the Hall angle in the normal state. However, because both theories assume pure materials these results are interesting but not surprising. The Hall angle results of Reed, Fawcett, and Kim (ref. 74) on high purity niobium (resistance ratio, $R_{300}/R_{4.2}=1550$) agree more closely with the Bardeen-Stephen prediction. However, other experiments (by Fiory and Serin) on niobium (resistance ratio, $R_{300}/R_{4.2}=3000$, refs. 75 and 76) pointed out the effects of pinning. Both theories assume that there is no pinning. Therefore, in order to distinguish between the two theories the effects of pinning must be eliminated. Fiory and Serin first proposed to do this by de-pinning the flux with a 20-kilohertz, 1.50×10^{-2} tesla magnetic field superimposed on a constant magnetic field. The direct current density used was 1.350×10^{7} amperes per square meter. They obtained results (ref. 75) which more closely agreed with the Bardeen-Stephens theory. In their second paper (ref. 76) they used direct current densities of 1.1×10^{8} amperes per square meter to overcome the pinning. Their results this time agreed with the Nozieres-Vinen prediction. By way of comparison, the maximum current density used by Reed, Fawcett, and Kim was 1.090×10^{7} amperes per square meter. Still another experiment performed on niobium by B. W. Maxwell (ref. 77) supports the Nozieres-Vinen model. Maxwell measured helicon resonance parameters in the mixed state. Relating these measurements to the Hall angle he found it to be field independent. The present experimental evidence seems to support the Nozieres-Vinen model when pinning effects are overcome, whereas the Bardeen-Stephens model applies when pinning effects are still effective. Nozieres and Vinen (ref. 70) suggest that another crucial experiment would be the measurement of the dispersion of helicon waves in very pure materials ($\omega_c\tau \gg 1$). The theoretical predictions are

$$\omega=\begin{cases} k^2\lambda^2\dfrac{eH}{mc} & \text{Nozieres-Vinen model} \\ k^2\lambda^2\dfrac{eH}{mc}\dfrac{H}{H_{c2}} & \text{Bardeen-Stephens model} \end{cases} \tag{131}$$

where ω is the frequency of the helicon waves. This experiment must await higher purities than are presently available.

RIGIDITY OF FLUX LATTICE

The Abrikosov flux structure has a rigidity that results from the repulsive force between flux lines. DeGennes (ref. 42) has derived the force between two vortex lines. He starts with the assumption of a modified London equation:

$$\boldsymbol{h}+\lambda^2(\nabla\times\nabla\times\boldsymbol{h})=\varphi_o[\delta(\boldsymbol{r}-\boldsymbol{r}_1)+\delta(\boldsymbol{r}-\boldsymbol{r}_2)] \tag{132}$$

The delta function terms are added to include the contributions to the field resulting from two flux lines at $\boldsymbol{r}_1$ and $\boldsymbol{r}_2$:

$$\boldsymbol{h}=\boldsymbol{h}_1(r)+\boldsymbol{h}_2(r) \tag{133}$$

The free energy of this system is given by equation (51), and equation (65) is

$$\begin{aligned}\boldsymbol{F}&=\frac{\lambda^2}{8\pi}\int \boldsymbol{h}\times(\nabla\times\boldsymbol{h})\cdot d\boldsymbol{\sigma}\\&=\frac{\lambda^2}{8\pi}\int (d\boldsymbol{\sigma}_1+d\boldsymbol{\sigma}_2)\cdot(\boldsymbol{h}_1+\boldsymbol{h}_2)\times(\nabla\times\boldsymbol{h}_1+\nabla\times\boldsymbol{h}_2)\end{aligned} \tag{134}$$

It is understood that the surface of integration is the cylindrical surface of the two cores ($|\boldsymbol{r}-\boldsymbol{r}_i|=\xi$). The indicated vector operations in the integrand of equation (134) result in eight terms:

$$\begin{aligned}\frac{\lambda^2}{8\pi}[\,&\int d\boldsymbol{\sigma}_1\cdot\boldsymbol{h}_1\times(\nabla\times\boldsymbol{h}_1)+\int d\boldsymbol{\sigma}_1\cdot\boldsymbol{h}_1\times(\nabla\times\boldsymbol{h}_2)+\int d\boldsymbol{\sigma}_1\cdot\boldsymbol{h}_2\times(\nabla\times\boldsymbol{h}_1)\\&+\int d\boldsymbol{\sigma}_1\cdot\boldsymbol{h}_2\times(\nabla\times\boldsymbol{h}_2)+\int d\boldsymbol{\sigma}_2\cdot\boldsymbol{h}_1\times(\nabla\times\boldsymbol{h}_1)\\&+\int d\boldsymbol{\sigma}_2\cdot\boldsymbol{h}_1\times(\nabla\times\boldsymbol{h}_2)+\int d\boldsymbol{\sigma}_2\cdot\boldsymbol{h}_2\times(\nabla\times\boldsymbol{h}_1)\\&+\int d\boldsymbol{\sigma}_2\cdot\boldsymbol{h}_2\times(\nabla\times\boldsymbol{h}_2)\,]\end{aligned} \tag{135}$$

The first term and the last term represent the self-energy (eq. (65)) of each vortex line. DeGennes assumes that the current $(\nabla\times\boldsymbol{h})$ at one vortex core due to the other vortex can be neglected. Therefore, in equation (135) the second, fourth, fifth, and seventh terms are dropped. The remaining two terms represent the interaction potential between the two flux lines U_{12}:

$$U_{12}=\frac{\lambda^2}{8\pi}\{\int[\boldsymbol{h}_1\times(\nabla\times\boldsymbol{h}_2)\cdot d\boldsymbol{\sigma}_2]+\int \boldsymbol{h}_2\times(\nabla\times\boldsymbol{h}_1)\cdot d\boldsymbol{\sigma}_1\} \tag{136}$$

From equation (70) and its general solution $K_o(x)$ the modified Bessel function of order zero,

$$|\nabla \times \boldsymbol{h}_2| = \frac{\varphi_o}{2\pi\lambda^2} \frac{1}{|\boldsymbol{r}-\boldsymbol{r}_2|} \tag{137}$$

and

$$h_{12} = h_1(\boldsymbol{r}_2) = \frac{\varphi_o}{2\pi\lambda^2} K_o\left(\frac{|\boldsymbol{r}_1-\boldsymbol{r}_2|}{\lambda}\right) \tag{138}$$

Therefore,

$$\int \boldsymbol{h}_1 \times (\nabla \times \boldsymbol{h}_2) \cdot d\boldsymbol{\sigma}_2 = \int \frac{\varphi_o}{2\pi\lambda^2} K_o\left(\frac{|\boldsymbol{r}_1-\boldsymbol{r}_2|}{\lambda}\right) \left\{\frac{\varphi_o}{2\pi\lambda^2} \frac{1}{|\boldsymbol{r}-\boldsymbol{r}_2|}\right\} |\boldsymbol{r}-\boldsymbol{r}_2| \, d\theta \tag{139}$$

$$\int \mathbf{h}_1 \times (\nabla \times \boldsymbol{h}_2) \cdot d\boldsymbol{\sigma}_2 = 2\pi \left(\frac{\varphi_o}{2\pi\lambda^2}\right)^2 K_o\left(\frac{|\boldsymbol{r}_1-\boldsymbol{r}_2|}{\lambda}\right) = \frac{\varphi_o^2}{2\pi\lambda^4} K_o\left(\frac{|\boldsymbol{r}_1-\boldsymbol{r}_2|}{\lambda}\right) \tag{140}$$

The other term in equation (136) gives an identical result. Therefore, the interaction energy is

$$U_{12} = \frac{\varphi_o^2}{8\pi^2\lambda^2} K_o\left(\frac{|\boldsymbol{r}_1-\boldsymbol{r}_2|}{\lambda}\right) \tag{141}$$

Substituting the field at vortex line 2 due to vortex line 1 (eq. (138)) into equation (141) results in

$$U_{12} = \frac{\varphi_o}{4\pi} h_{12} \tag{142}$$

The modified Bessel function

$$K_o\left(\frac{|\boldsymbol{r}_1-\boldsymbol{r}_2|}{\lambda}\right) \to \sqrt{\frac{\pi\lambda}{2r_{12}}} e^{-r_{12}/\lambda}$$

for large r_{12} and

$$K_o\left(\frac{|\boldsymbol{r}_1-\boldsymbol{r}_2|}{\lambda}\right) \to \ln\left(\frac{\lambda}{r_{12}}\right)$$

for small r_{12}. Figure 26 shows a plot of $K_o(r_{12}/\lambda)$: note that it becomes very small at something less than $r_{12}/\lambda = 3$. The force exerted by one flux line on the other can be calculated from the potential U_{12}:

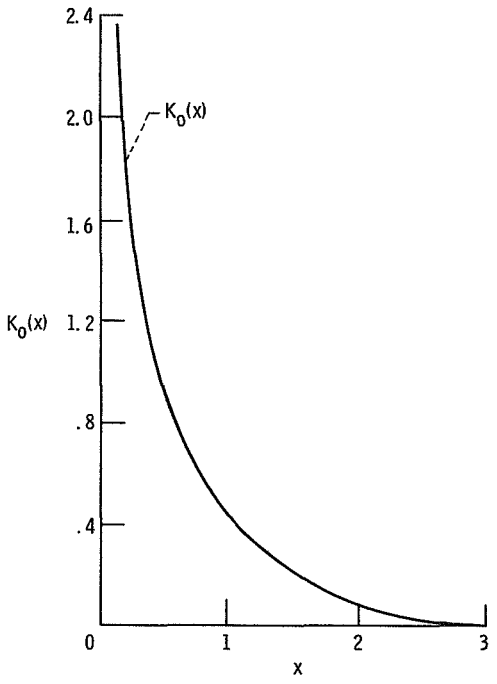

FIGURE 26.—Modified Bessel function plotted against its argument (ref. 78).

$$f_{2x}=-\frac{\partial U_{12}}{\partial x}=-\frac{\varphi_o}{4\pi}\frac{\partial h_{12}}{\partial x} \tag{143}$$

where $x=r_{12}/\lambda$ is taken as one axis in a rectangular coordinate system. DeGennes then identifies $\partial h_{12}/\partial x$ as $-(4\pi/c)j_y$, which is just the current density predicted by Maxwell's equation $\nabla\times\boldsymbol{H}=(4\pi/c)\boldsymbol{J}$. This gives a force

$$f_{2x}=\frac{\varphi_o}{c}j_y \tag{144}$$

which is a Lorentz type force. The flux lines are therefore forced apart, but they cannot leave the superconductor because if they did more energy would be required. The additional energy would be needed to create surface currents large enough to exclude more magnetic flux. The repulsive force between flux lines therefore results in rigidity of the flux lattice. Kim, Hempstead, and Strnad's theory (refs. 49 and 53) of flux flow implicitly assumes that the entire flux lattice moves as a unit.

DeGennes' result (eq. (144)) is essentially valid when the flux lines are more than a penetration depth apart. If the flux lines are less than a

penetration depth apart, then all the terms of equation (135) which were discarded must be included.

VISCOUS DRAG FORCE

In the section on FLUX FLOW, a viscous drag force on the moving flux lattice was postulated (p. 33). It was needed to explain why the flux lattice does not accelerate indefinitely. The proposed mechanisms for the viscous drag force are discussed in this section. In actuality some combination of these effects, perhaps even all of them, may contribute to the viscous drag force

$$\boldsymbol{f}=\eta \boldsymbol{v}_L \tag{145}$$

Before proceeding with the various models for the viscous drag force, it is useful to derive an empirical expression for the viscosity parameter η. This result can be compared with the results of the various theories to evaluate them. Dividing equation (105) by $\boldsymbol{J}$ yields the flux flow resistivity

$$\rho_f=\frac{\varphi_o}{\eta c^2}H \tag{146}$$

Then, substituting this for ρ_f in the law of corresponding states (eq. (98)) and solving for η yield

$$\eta_{empirical}=\frac{\varphi_o H_{c2}(0)}{\rho_n c^2} \tag{147}$$

Equation (147) can be written in several alternate forms (ref. 53) using the expression for $H_{c2}(0)$ derived by Maki (refs. 79 and 80) and using several relationships between the fundamental parameters:

$$\eta_{empirical}=\pi\hbar N(0)\Delta_o \tag{148a}$$

$$=6.4\times 10^{-12}\gamma T_c \tag{148b}$$

or

$$=\frac{3\sigma_n\varphi_0^2}{2\pi^2c^2\xi^2} \tag{148c}$$

where $N(0)$ is the normal state density of electron states, γ is the electronic specific heat constant, and σ_n is the normal conductivity. Equation (148) points out that $\eta_{empirical}$ depends only on $N(0)$ and Δ_o. Notably it is independent of the mean free path of the electrons.

The first viscosity mechanism to be discussed is normal eddy-current damping, which was first proposed by Volger, Staas, and Van Vijfeijken (ref. 81). If equation (145) is substituted into equation (104) for $\boldsymbol{F}_L$, the power dissipated is

$$P=n\eta v_L^2 \tag{149}$$

At low temperatures where the only normal electrons are in the core, the total power dissipated should be equal to the number of cores n times the power dissipated in each core:

$$P=n\int\int\sigma E^2 dxdy \tag{150}$$

As mentioned previously, when flux moves there is an associated electric field (eq. (115)). When the applied current and field are perpendicular, $\boldsymbol{E}=-(v_L/c)H$. An expression for η is obtained by substituting this into equation (150) on the right, substituting equation (149) into equation (150) on the left, and solving for η:

$$\eta=\frac{1}{\rho_n c^2}\int\int H_{core}^2\, dxdy=\frac{\pi\xi^2 H_{core}^2}{\rho_n c^2} \tag{151}$$

Maki's expression (refs. 70 and 71) for $H_{c2}(0)$ can be manipulated into the form

$$H_{c2}(0)=\frac{3\varphi_o}{2\pi^2\xi^2} \tag{152}$$

Then if equation (151) is multiplied and divided by H_{c2}^2

$$\eta=\frac{3\varphi_o}{2\pi\rho_n c^2}H_{c2}(0)\left[\frac{H_{core}}{H_{c2}(0)}\right]^2 \tag{153}$$

Kim, Hempstead, and Strnad (ref. 53) have pointed out that equation (153) is only equal to equation (147) near H_{c2}, and the η given by the normal eddy-current damping model is always much less than the empirical value. Therefore, this mechanism may well exist, but it is by no means the primary source of viscosity.

Stephen and Bardeen (ref. 82) proposed a cycloidal damping scheme. They pointed out that if a flux line does not move too fast, the entire vortex structure moves as a unit. Under these conditions the electrons in the vortex move in a circular path when the flux line is stationary $\boldsymbol{v}_s(\boldsymbol{r})$. But when the vortex is moving, the electrons move on a cycloidal

path $\boldsymbol{v}_s(\boldsymbol{r}-\boldsymbol{v}_L t)$. This situation is somewhat analogous to the motion of an electron in crossed electric and magnetic fields. Stephen and Bardeen argue that likewise in the case of vortex motion an electric field must be present to exert the force that results in the cycloidal motion. If $\boldsymbol{R}=(\boldsymbol{r}-\boldsymbol{v}_L t)$, the acceleration experienced by the vortex electrons is

$$\frac{d\boldsymbol{v}_s(\boldsymbol{R})}{dt}=\nabla\,\boldsymbol{v}_s(\boldsymbol{R})\cdot\frac{\partial \boldsymbol{R}}{\partial t}=\nabla\,\boldsymbol{v}_s(\boldsymbol{R})\cdot\left(\frac{\partial \boldsymbol{r}}{\partial t}-t\,\frac{\partial \boldsymbol{v}_L}{\partial t}-\boldsymbol{v}_L\right) \tag{154}$$

If the flux flow motion is steady state, $\partial \boldsymbol{v}_L/\partial t=0$. Because the vortex is assumed to be rigid, $\partial \boldsymbol{r}/\partial t=0$. The electric field associated with the force on the vortex electrons is

$$\left(\frac{e}{m}\right)\boldsymbol{E}=(\boldsymbol{v}_L\cdot\nabla)\boldsymbol{v}_s \tag{155}$$

A detailed analysis of this electric field in the region of the vortex core indicates that inside the core the field is constant and equal to

$$\boldsymbol{E}_c=\frac{\boldsymbol{v}_L}{e}\left(\frac{\partial p}{\partial r}\right)_r \tag{156}$$

where p is the momentum of the paired electrons defined by the quantum condition

$$2\oint \boldsymbol{p}\cdot d\boldsymbol{l}=h \tag{157}$$

Then

$$p=\frac{\hbar}{2\xi} \tag{158}$$

and ξ is the radius of the circular path of integration. Differentiating equation (158) and substituting into equation (156) gives

$$\boldsymbol{E}_c=-\frac{\boldsymbol{v}_L}{e}\,\frac{\hbar}{2\xi^2} \tag{159}$$

Now a viscosity parameter can be calculated by equating the total rate of dissipation to the dissipation in the core:

$$\eta v_L^2=\pi\xi^2\sigma_n(E_c^2) \tag{160}$$

Then if equation (159) is substituted into equation (160), solving for η yields

$$\eta = \frac{\pi \sigma_n \hbar^2}{e^2 4\xi^2} \tag{161}$$

Multiplying and dividing by $\varphi_0^2 = h^2c^2/4e^2$ in equation (161) gives

$$\eta = \frac{\sigma_n \varphi_0^2}{4\pi c^2 \xi^2} \tag{162}$$

Equation (162) is $\pi/6$, or roughly one-half the empirical viscosity (eq. (148c)).

Tinkham (ref. 83) has suggested an additional source of damping. It results from the variation of ψ when the flux lines move. At a point inside a material which is in the flux flow state, the superconducting wave function oscillates between ψ_o (superconducting state) and 0 (normal state) as normal cores pass through the point. Tinkham approximates the frequency of this oscillation by $\omega \cong v_L/\xi$. The superconducting electrons thus gain and lose the condensation energy $\omega/2\pi$ times each second. If the instantaneous value of ψ lags behind the value appropriate for the moving Abrikosov structure by a time τ, then a fraction $\omega\tau$ of the energy is dissipated. This energy goes to the production and/or heating of normal electrons. Tinkham approximates the Gibbs free energy by the second term of equation (33), which is the Ginzburg-Landau expression. Then equation (163) is obtained by multiplying and dividing the approximation by ψ_δ^2 (eq. (36)):

$$G = \frac{H_c^2(T)}{4\pi} \left| \frac{\psi_o(H, T)}{\psi_o(0, T)} \right|^2 \tag{163}$$

For convenience,

$$\chi^2 = \left| \frac{\psi_o(H, T)}{\psi_o(0, T)} \right|^2$$

The power dissipated per unit length is the amount of energy lost per cycle times the number of cycles:

$$P = (G\omega\tau)\omega\pi\xi^2 = \left[\frac{H_c^2(T)}{4\pi} \chi^2\right] \frac{v_L^2}{\xi^2} 2\pi\xi^2 \tag{164}$$

Again the plan is to set the power dissipated to ηv_L^2 and solve for η. But before doing this Tinkham approximates χ^2 and τ. He assumes that the

relaxation time is limited by the uncertainty principle

$$\tau=\frac{\hbar}{\Delta}=\frac{\hbar}{\Delta_o}\frac{(1+t^2)}{(1-t^2)} \tag{165}$$

where $t=T/T_c$ or the reduced temperature. He further approximates χ^2 by

$$\chi^2=1-b^2 \tag{166}$$

where $b=B/H_{c2}$. Then substituting equations (165) and (166) into equation (164), setting P equal to ηv_L^2, η can be solved for

$$\eta=\tau\frac{H_c^2}{4}\chi^2(H, T)=\frac{\hbar H_c^2}{4\Delta_o}(1-b^2)\frac{(1+t^2)}{(1-t^2)} \tag{167}$$

This expression is quite different from $\eta_{empirical}$. It has both a temperature and magnetic field dependency. However, the temperature and magnetic field dependence in $\eta_{empirical}$ was ignored. Therefore, it is possible that equation (167) is, in fact, more exact. If equation (167) is substituted into equation (146),

$$\rho_f=\frac{4H\varphi_o}{c^2\tau H_c^2\chi^2} \tag{168}$$

Then for dirty (mean free path $\ll \xi_o$) superconductors

$$\frac{1}{\rho_n}=\frac{c^2}{4\pi}\frac{h}{\Delta_o\lambda^2(0)}$$

$$H_{c2}(T)=\frac{4\pi H_{cb}^2\lambda^2(T)}{\varphi_o}$$

and

$$\lambda_L(0)=\left(\frac{mc^2}{4\pi ne^2}\right)^{1/2}$$

Substituting these into equation (168) gives

$$\frac{\rho_f}{\rho_n}=\frac{4}{\pi}\frac{H}{H_{c2}(T)}\frac{\hbar}{\Delta_o\tau(T)}\frac{\lambda^2(T)}{\lambda^2(0)}\frac{1}{\chi^2(H, T)} \tag{169}$$

If $\lambda^2(0)/\lambda^2(T)$ is set equal to $(1-t^4)$ and equations (165) and (166) are

substituted into (169),

$$\frac{\rho_f}{\rho_n}=\frac{4}{\pi}\frac{1}{(1+t^2)}\frac{b}{(1-b^2)} \tag{170}$$

Tinkham (ref. 83) then adds this to his own generalized version of the normal eddy current damping model and obtains

$$\frac{\rho_f}{\rho_n}=\frac{b}{(1+t^2)(1-b^2)+b^2+(b-b^2)t} \tag{171}$$

Note that at $t=0$, $\rho_f/\rho_n=H/H_{c2}$ and at $H=H_{c2}$, $\rho_f/\rho_n=1$. This relation can be compared directly with the experimental results (see fig. 27). The agreement is remarkably good, especially at low temperatures.

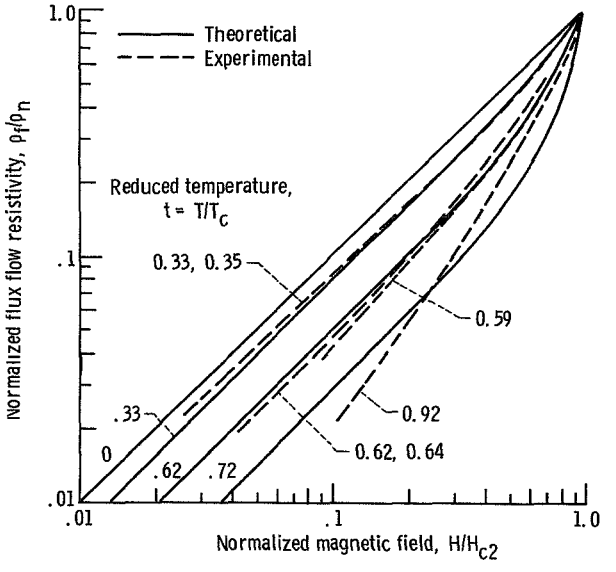

FIGURE 27.—Flux flow resistivity normalized to normal resistivity is plotted against applied magnetic field normalized to upper critical field H_{c2}. Tinkham's (ref. 83) results are compared with experimental results. (Temperature in Kelvin degrees represented by T.)

It has been suggested by Kim, Hempstead, and Strnad that the mechanisms of Bardeen-Stephen and Tinkham are independent (ref. 53). Their relationship may be better understood when experiments are performed in sufficiently clean materials. The Bardeen-Stephen model should be dependent on the mean free path, because it depends on collisions in

the vortex core. The Tinkham result is independent of mean free path. Both predictions are the correct order of magnitude to explain the experimental results.

FLUX PINNING MECHANISMS

In the FLUX FLOW section, the onset of flux flow was described. When the Lorentz force is sufficiently large the flux lattice moves and a voltage is observed. It is thought that a minimum Lorentz force is necessary to overcome the pinning forces exerted by crystal imperfections on the flux lines. The nature of these pinning forces is discussed in this section. The primary sources of pinning are thought to be dislocations and impurity atoms. Figure 28 attempts to show schematically several different types of pinning mechanisms. In sintered materials such as

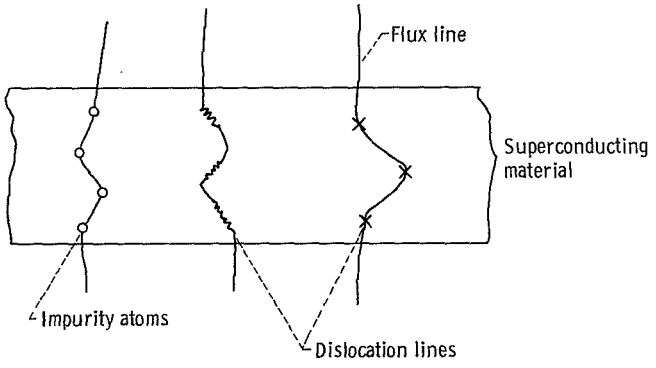

FIGURE 28.—Cross-sectional view of three different pinning mechanisms.

Nb_3Sn, where the sintering is incomplete, precipitates and cavities are thought to be the most important pinning mechanism (ref. 84). A flux line will become entwined in the defects (fig. 28) such as to minimize its energy taking account of the distance between flux lines and the size and density of the impurity atoms and cavities. Friedel, DeGennes, and Matricon (ref. 85) considered the case where one line is pinned by each cavity. They estimate the pinning force F_p to be

$$F_p = \left(\frac{\varphi_o}{4\pi\lambda}\right)^2 \ln\left(\frac{d'}{\xi_o}\right) \tag{172}$$

by equating F_p to the line energy (eq. (72)) and setting $\lambda = d'$, the distance between two pinning sites. If the density of cavities and/or precipitates

is such that it becomes likely that each flux line is pinned by more than one cavity, then presumably F_p should be divided by the number of cavities per line. At magnetic fields near H_{c2} the situation becomes more complicated. If the cavity radii are large enough and the distance between flux lines is small enough, then it becomes almost impossible to assign the pinning sites to particular flux lines. Complicating the problem still further is that the flux lines form into bundles. So if a bundle is pinned the force on the bundle is the composite Lorentz force on all the flux lines in the bundle. Under certain circumstances it may be energetically more favorable for the bundle to fragment rather than remain pinned. The flexibility of the flux lines also decreases at higher magnetic fields because of the repulsive forces between flux lines. Therefore, flux lines cannot bend to contact pinning sites.

The cavity pinning mechanism has also been studied by Silcox and Rollins (ref. 86). Silcox and Rollins determined the interaction potential between nearest neighbors empirically from magnetization measurements (refs. 87 and 88) to be

$$U(a)=\frac{\varphi_0^2}{12\pi\sqrt{3}\left(\frac{H_{c2}}{H_{c2}-H_{c1}}\right)a^2} \tag{173}$$

where a is the nearest-neighbor distance between flux lines. Then they assumed a density of pinning sites and equated the force of each pinning site to $H_{c1}\varphi_o/4\pi$. Using these assumptions they calculated the magnetic induction and the associated magnetization curve. Their results showed increasing hysteresis with increasing defect content. These results were very similar to the experimental results of Livingston and Swartz (refs. 87 and 88). Narlikar and Dew-Hughes (ref. 89) found that magnetic hysteresis in Nb was very sensitive to the dislocation density. Webb (ref. 90) calculated the pinning force on an infinitely long flux line due to one screw dislocation. He assumed that the nonuniform stress field of a dislocation provides the pinning mechanism. He calculated that in Nb with a dislocation density of 10^{14} per square meter, the pinning force would be 2×10^{-6} newton per meter. Yamafuji and Irie (ref. 91) have criticized Webb's calculation for assuming static conditions and for ignoring the lattice energy of the Abrikosov structure. They analyzed the case of a linear flux lattice moving with a constant velocity in the pinning potential shown in figure 29. They also assume that the individual flux lines in the lattice are displaced from their equilibrium position as the line moves through the potential well. The displacement from equilibrium is denoted by Δx. If the deformation results from a Hooke's law force, then the equation of motion is

$$M\Delta\ddot{x}+\eta\Delta\dot{x}+k\Delta x=-\frac{dU_{pf}}{dx} \tag{174}$$

where M is an effective mass per unit length, η the viscosity parameter, and k a restoring force constant. Considering the energy lost as a flux line moves past a pinning site yields a pinning force

$$f_p=(-k\Delta x) \tag{175}$$

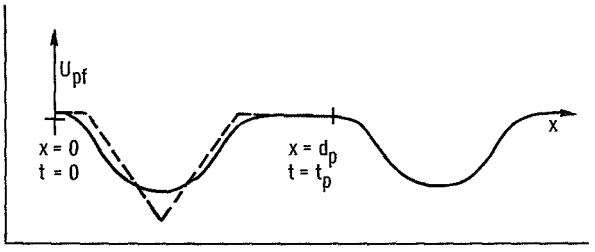

FIGURE 29.—Pinning site potential assumed by Yamafuji and Irie (ref. 91).

As the flux lattice moves past a particular pinning site, it is distorted. When the flux line is pulled free of the pinning site the deformation energy is transferred to vibrational energy of the crystal lattice. The vibrational energy in turn is dissipated to the viscous medium. Recently the present status of the relationship between critical current density and the pinning site has been reviewed by Livingston (ref. 92).

PRESENT SITUATION AND UNSOLVED PROBLEMS

In recent years considerable progress has been made toward a thorough understanding of the mixed state of superconductors. The present understanding is, however, far from complete. The brilliant experiments of Trauble and Essmann have proved the existence of the Abrikosov lattice. The flux creep theory of Anderson and Kim is in satisfactory agreement with the experimental results. Kim, Hempstead, and Strnad have correlated the voltage—current—magnetic field relations of type II superconductors by experiment and analysis. Their flux motion hypothesis and the law of corresponding states are in agreement with a considerable amount of experimental results. The motion of flux lines has been substantiated by the experiments of Hans Meissner. The existence of an associated voltage has been affiirmed by Pearl's experiments, and Goodman has derived the flux flow voltage from the Ginzburg-

Landau equations. The voltage is found to be the voltage that results from a Lorentz transformation between a moving system and a stationary system. The theoretical analyses of Bardeen-Stephen and Nozieres-Vinen have suggested possible mechanisms for the phenomena of flux flow. Several mechanisms have been suggested to explain the viscous drag postulated by Kim, Hempstead, and Strnad. The results of Tinkham's oscillating-wave-function damping scheme are extremely close to experimental results.

As impressive as the rate of progress toward a complete understanding of the mixed state has been, several areas need further theoretical and experimental analysis. The flux flow state must be incorporated into either a time-dependent Ginzburg-Landau theory or a still more general theory. Attempts toward a time-dependent theory have been made by Stephen and Suhl (ref. 93) and by Schmid (ref. 94). Schmid's solution incorporates a relaxation time for the order parameter that is similar to Tinkham's (ref. 83). At the Stanford superconductivity conference John Bardeen reported on his attempts to provide general solutions for superconductors where the energy gap parameter varies in space and time (ref. 95).

The experiments of Trauble and Essmann (ref. 48) proved that the mixed state is composed of individual flux quanta. More recent experiments (refs. 96 to 99) utilizing these same techniques have produced results which indicate that the triangular lattice of flux lines is not always found. Much of this evidence supports an intermediate state in type II superconductors. Essmann (ref. 100) interprets these results as an indication of an attractive interaction between flux lines.

Trauble and Essmann (ref. 96) have also studied flux flow in lead foils. They applied magnetic field and current and deposited small magnetic particles onto the sample. With no transport current through the film they found a flux structure consisting of flux bundles of about 50 quanta. When a field of 6.0×10^{-3} tesla and a current density of 1.2×10^{8} amperes per square meter was applied, the sample was in the flux flow state. Under these conditions an evaporation time of about 1 second produced the picture shown in figure 30. The dark areas correspond to the regions of the sample that the flux lines moved through. The result shown in figure 30 is unexpected. If the flux lattice moved through the sample as a rigid entity the sample surface would be expected to be blackened evenly. Instead, figure 30 shows that the flux lines flow along specific paths. Clearly this experimental observation is contrary to the Kim, Hempstead, and Strnad flux flow theory, which assumes that all the flux lines move together.

There is other evidence which points to limitations of the flux flow model. Hans Meissner has observed that when the current reaches a

FIGURE 30.—Electron microscope picture of flux flow in lead foils (ref. 96). Magnetic field intensity, $H = 6.0 \times 10^{-3}$ tesla; current density, $J = 1.2 \times 10^{8}$ amperes per square meter.

certain value he can no longer observe flux moving across the sample. This current level corresponds to flux flow velocities equal to the velocity of sound. Since superconductivity in the Bardeen-Cooper-Schrieffer formulation is a phonon coupling of electrons, it would not be surprising at all if the flux lines had some maximum velocity. These ideas were presented by Meissner (ref. 57). It has also been observed by Hudson and Jirberg (ref. 101) that in niobium the voltage is never directly proportional to the current (fig. 31). This is contrary to the prediction of Kim, Hempstead, and Strnad (eq. (105)). If the number of flux lines in motion varies, it is possible to explain almost any nonlinear flux flow voltage. Trauble and Essmann have in fact observed instances where part of the flux moves while another part is held stationary by pinning.

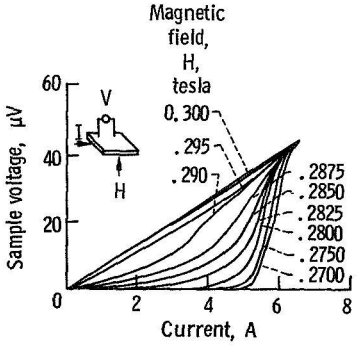

FIGURE 31.—Resistive transition near H_{c2} (ref. 101).

APPENDIX A

PLOTS OF CRITICAL FIELD AS FUNCTION OF TEMPERATURE

The curves below are plots of critical magnetic field as a function of temperature for several elements. The source of the curves is reference 102.

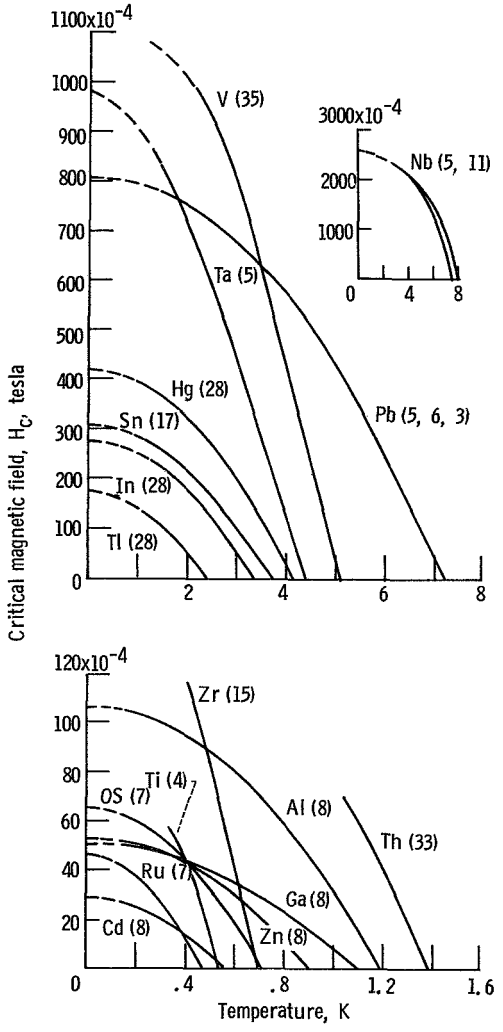

FIGURE 32. — Critical field as function of temperature.

APPENDIX B

PHOTOGRAPHS OF INTERMEDIATE STATE

The intermediate state has been optically observed using an experimental technique that takes advantage of the Faraday rotation effect. Some pictures taken by Faber (ref. 16) are presented in this appendix. In these pictures of an aluminum plate the dark areas are the superconducting regions in the materials.

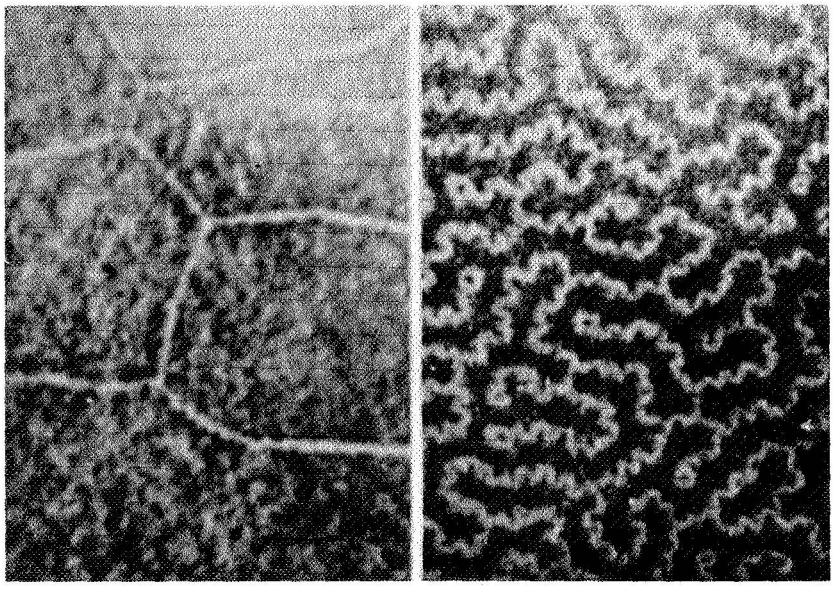

(a) $H = 0$ (trapped flux). (b) $H = 0.27\ H_c$.

FIGURE 33. — Intermediate state.

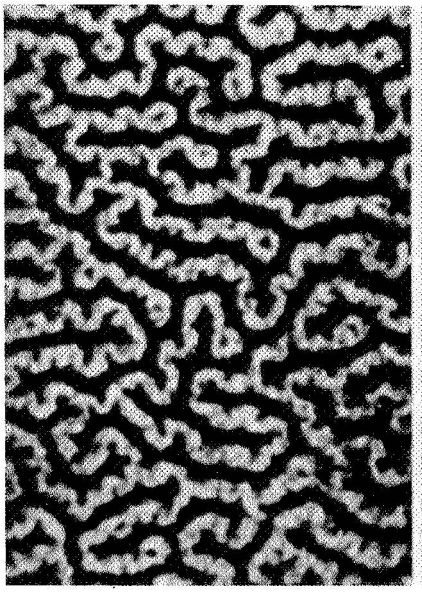

(c) $H = 0.38\ H_c$.

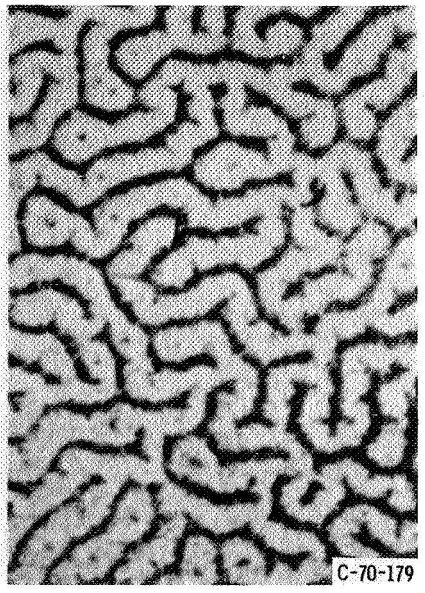

(d) $H = 0.53\ H_c$.

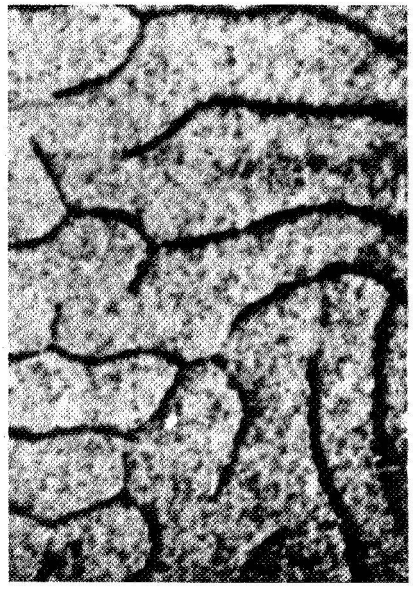

(e) $H = 0.79 H_c$.

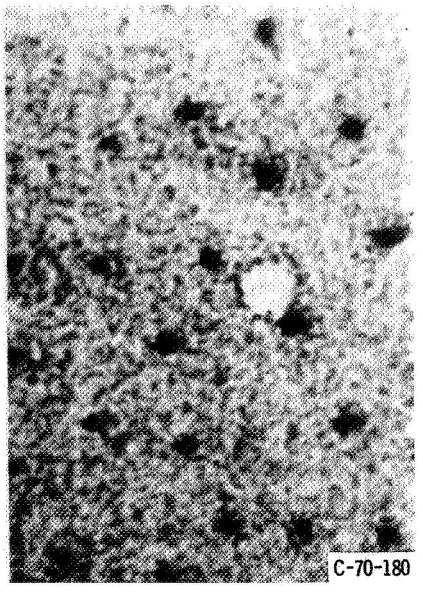

(f) $H = 0.9\ H_c$.

FIGURE 33. – Concluded.

APPENDIX C

INTEGRAL TRANSFORMATION

The purpose of this appendix is to demonstrate the integral transformation mentioned on page 32. The integral under discussion is

$$lZ = \int_{(r>\xi)} dr \, \frac{1}{8\pi} \left[h^2 + \lambda_L^2 (\nabla \times \boldsymbol{h})^2\right] \tag{C1}$$

Integration can be performed if the integral is first transformed to a surface integral. The necessary transformation can be derived from the divergence theorem and the vector identity:

$$\nabla \cdot (\boldsymbol{A} \times \boldsymbol{B}) = \boldsymbol{B} \cdot (\nabla \times \boldsymbol{A}) - \boldsymbol{A} \cdot \nabla \times \boldsymbol{B} \tag{C2}$$

$$\int_s d\boldsymbol{\sigma} \cdot (\boldsymbol{A} \times \boldsymbol{B}) = \int dr (\nabla \cdot (\boldsymbol{A} \times \boldsymbol{B})) = \int dr (\boldsymbol{B} \cdot \nabla \times \boldsymbol{A}) - \int dr (\boldsymbol{A} \cdot \nabla \times \boldsymbol{B}) \tag{C3}$$

If $\boldsymbol{A} = \nabla \times \boldsymbol{h}$ and $\boldsymbol{B} = \boldsymbol{h}$, then

$$\int_s d\boldsymbol{\sigma} \cdot ((\nabla \times \boldsymbol{h}) \times \boldsymbol{h}) = \int dr (\boldsymbol{h} \cdot \nabla \times \nabla + \boldsymbol{h}) - \int dr (\nabla \times \boldsymbol{h}) \cdot (\nabla \times \boldsymbol{h}) \tag{C4}$$

Recognizing the term with the $(\nabla \times \boldsymbol{h})^2$ integrand as the second term in equation (64) gives

$$lZ = \frac{1}{8\pi} \left\{ \int dr \, h^2 - \lambda^2 \int d\boldsymbol{\sigma} \cdot [(\nabla \times \boldsymbol{h}) \times \boldsymbol{h}] + \lambda^2 \int dr [\boldsymbol{h} \cdot (\nabla \times \nabla \times \boldsymbol{h})] \right\} \tag{C5}$$

$$lZ = \frac{1}{8\pi} \left(\int dr \, \{h^2 + \lambda^2 [\boldsymbol{h} \cdot (\nabla \times \nabla \times \boldsymbol{h})]\} - \lambda^2 \int d\boldsymbol{\sigma} \cdot [(\nabla \times \boldsymbol{h}) \times \boldsymbol{h}] \right) \tag{C6}$$

Then recognizing the integrand of the volume integrand as the London equation (eq. (6)) yields

$$lZ = \frac{\lambda^2}{8\pi} \int d\boldsymbol{\sigma} \cdot [\boldsymbol{h} \times (\nabla \times \boldsymbol{h})] \tag{C7}$$

APPENDIX D

DERIVATION OF EQUATION (76)

This appendix shows the steps necessary to derive equation (76) from equation (75). In order to get started several equations must be borrowed from the Bardeen-Cooper-Schrieffer theory (refs. 26 and 27):

$$\left.\begin{aligned} -H_c &= 2\pi^{1/2}N^{1/2}\Delta \\ \Delta &= \frac{\hbar v_F}{\pi\xi} \end{aligned}\right\} \tag{D1}$$

where N is the density of states at the Fermi energy per unit (energy cm^3). Substituting for Δ gives

$$H_c = 2\pi^{1/2}N^{1/2}\frac{\hbar v_F}{\pi\xi} \tag{D2}$$

Dividing equation (D1) into equation (75) gives

$$\frac{H_{c1}}{H_c} = \frac{\frac{\varphi_o}{4\pi}\pi}{2\pi^{1/2}N^{1/2}\hbar v_F}\frac{\xi}{\lambda^2}\ln\frac{\lambda}{\xi} \tag{D3}$$

Substituting $\varphi_o = ch/2e$ into equation (D3) yields

$$\frac{H_{c1}}{H_c} = \frac{\pi^{1/2}c}{8N^{1/2}ev_F}\frac{\xi}{\lambda^2}\ln\frac{\lambda}{\xi} \tag{D4}$$

Then substituting $\lambda = (mc^2/4\pi ne^2)^{1/2}$ for one of the λ's gives

$$\frac{H_{c1}}{H_c} = \frac{\pi}{4m^{1/2}v_F}\frac{n^{1/2}}{N^{1/2}}\frac{\xi}{\lambda}\ln\frac{\lambda}{\xi} \tag{D5}$$

Finally, replacing N with $m^2v_F/2\pi^2\hbar^3$, $\kappa = \lambda/\xi$ and v_F with $\hbar/m(3\pi^2n)^{1/3}$ can give the desired result:

$$H_{c1} = \frac{\pi}{\sqrt{24}}\frac{H_c}{\kappa}\ln\kappa \tag{D6}$$

TABLE I.—SUPERCONDUCTING PARAMETERS

Element	Penetration depth, $\lambda(0)$, Å	Energy gap, $2\Delta(0)$	Coherence length, ξ_o, Å
Al	500	0.34×10^{-3}	16 000
Cd	1300		7 600
Hg	380 to 450	1.65	
In	640	1.05	4 400
Pb	390	2.67	830
Sn	510	1.15	2 300
Tl	920		
V			
Nb	440	3.05	380
Ta		1.40	
NbTi, NbZr, Nb_3Sn	These materials vary considerably with composition (refs. 103 and 104)		

REFERENCES

1. ONNES, H. KAMERLINGH: Disappearance of the Electrical Resistance of Mercury at Helium Temperatures. Proc. K. Akad. Wetenschappen, vol. 14, June 23, 1911, pp. 113–115.
2. ROBERTS, B. W.: Superconductive Materials and Some of Their Properties. Rep. 63–RL–3252M, General Electric Co., Mar. 1963.
3. ONNES, H. K.: Further Experiments with Liquid Helium. VII. The Potential Difference Necessary for the Flow of an Electric Current Through Mercury Below 4.19° K. Verslag Akad. Wetenschappen, 1913, pp. 1284–1305.
4. ONNES, H. KAMERLINGH: Experiments with Liquid Helium. The Electrical Resistance, etc. VIII. The Sudden Disappearance of the Ordinary Resistance of Tin and Super-Conductive State of Lead. Proc. K. Akad. Wetenschappen, vol. 16, 1914, pp. 673–688.
5. ONNES, H. KAMERLINGH: Further Experiments with Liquid Helium. I. The Hall Effect and the Change of Resistance in a Magnetic Field at Low Temperatures. IX. Occurrence of Galvanic Resistance in Super-Conductors, When Brought into a Magnetic Field, at a Threshold Value of the Field. Verslag Akad. Wetenschappen, vol. 22, 1914, pp. 1027–1033.
6. TUIJN, W.; AND ONNES, H. KAMERLINGH: The Disturbance Produced in Superconductivity by Magnetic Fields and Currents. Silsbee's Hypothesis. Arch. Néerland, Sci. IIIA, vol. 10, 1927, pp. 224–258.
7. DE HAAS, W. J.; AND VOOGD, J.: Electrical Resistance at Low Temperatures and Effect of Magnetic Field. Proc. K. Akad. Amsterdam, vol. 34, no. 1, 1931, pp. 51–55.
8. SILSBEE, F. B.: Electrical Conduction in Metals at Low Temperatures. J. Wash. Acad., vol. 6, 1916, pp. 597–602.
9. DE HAAS, W. J.; AND VOOGD, J.: Steepness of the Transition Curve of Superconductors. Proc. K. Akad. Amsterdam, vol. 34, no. 2, 1931, pp. 192–203.
10. GRASSMANN, P.: Microresistance of Superconductors. Physik. Z., vol. 37, 1936, pp. 569–578.
11. FILE, J.; AND MILLS, R. G.: Observation of Persistent Current in a Superconducting Solenoid. Phys. Rev. Letters, vol. 10, no. 3, Feb. 1, 1963, pp. 93–96.
12. MEISSNER, W.; AND OCHSENFELD, R.: Ein Neuer Efekt bei Eintritl der Supraleitfähigkeit. Naturwiss enschaften, vol. 21, 1933, pp. 787–788.
13. LYNTON, ERNEST A.: Superconductivity. John Wiley & Sons, Inc., 1962.
14. NEWHOUSE, VERNON L.: Applied Superconductivity. John Wiley & Sons, Inc., 1964.
15. ALERS, P. B.: Structure of Intermediate State in Superconducting Lead. Phys. Rev., vol. 105, no. 1, Jan. 1, 1957, pp. 104–108.
16. FABER, T. E.: The Intermediate State in Superconducting Plates. Proc. Roy. Soc. (London), Ser. A., vol. 248, no. 1255, Dec. 9, 1958, pp. 460–481.
17. BECKER, R.; HELLER, G.; AND SAUTER, F.: Current Distribution in a Supraconducting Sphere. Zeits. f. Physik, vol. 85, no. 11–12, Oct. 14, 1933, pp. 772–787.
18. LONDON, F.; AND LONDON, H.: The Electromagnetic Equations of the Supraconductor. Proc. Roy. Soc. (London), Ser. A., vol. 149, no. 866, Mar. 1, 1935, pp. 71–88.
19. GORTER, C. J.: Theory of Superconductivity. Nature, vol. 132, 1933, p. 931.
20. GORTER, C. J.; AND CASIMIR, H.: Superconductivity. I. Physica, vol. 1, 1934, pp. 306–320.

21. KEELEY, T. C.; MENDELSSOHN, K.; AND MOORE, J. R.: Experiments on Supraconductors. Nature, vol. 134, 1934, p. 773.
22. MENDELSSOHN, K.; AND MOORE, J. R.: Magneto-Caloric Effect in Supraconducting Tin. Nature, vol. 133, 1934, p. 413.
23. KEESOM, W. H.; AND KOK, J. A.: Specific Heat of Thallium at Liquid Helium Temperatures. Physica, vol. 1, Jan. 1934, pp. 175–181.
24. MENDELSSOHN, K.; AND MOORE, J. R.: Specific Heat of a Supraconducting Alloy. Proc. Roy. Soc. (London), Ser. A, vol. 151, no. 873, Sept. 2, 1935, pp. 334–341.
25. GOODMAN, B. B.: Simple Model for the Magnetic Behavior of Superconductors of Negative Surface Energy. Phys. Rev. Letters, vol. 6, no. 11, June 1, 1961, pp. 597–599.
26. FRÖHLICH, H.: Theory of the Superconducting State. I. The Ground State at the Absolute Zero of Temperature. Phys. Rev., vol. 79, no. 5, Sept. 1, 1950, pp. 845–856.
27. MAXWELL, EMANUEL: Isotope Effect in Superconductivity of Mercury. Phys. Rev., vol. 78, no. 4, May 15, 1950, p. 477.
28. REYNOLDS, C. A.; SERIN, B.; WRIGHT, W. H.; AND NESBITT, L. B.: Superconductivity of Isotopes of Mercury. Phys. Rev., vol. 78, no. 4, May 15, 1950, p. 487.
29. BARDEEN, J.; COOPER, L. N.; AND SCHRIEFFER, J. R.: Microscopic Theory of Superconductivity. Phys. Rev., vol. 106, no. 1, Apr. 1, 1957, pp. 162–164.
30. BARDEEN, J.; COOPER, L. N.; AND SCHRIEFFER, J. R.: Theory of Superconductivity. Phys. Rev., vol. 108, no. 5, Dec. 1, 1957, pp. 1175–1204.
31. PIPPARD, A. B.: The Surface Impedance of Superconductors and Normal Metals at High Frequencies. V. Analysis of Experimental Results for Superconducting Tin. Proc. Roy. Soc. (London), Ser. A, vol. 203, no. 1073, Sept. 22, 1950, pp. 195–210.
32. ABRIKOSOV, A. A.: On the Magnetic Properties of Superconductors of the Second Group. Soviet Phys.—JETP, vol. 5, no. 6, Dec. 15, 1957, pp. 1174–1182.
33. LONDON, FRITZ: Superfluids. Vol. 1. Second ed., Dover Publ., Inc., 1961.
34. GINZBURG, V. L.; AND LANDAU, L. D.: On the Theory of Superconductivity. Zh. Eksper. Teoret. Fisiki, vol. 20, no. 12, 1950, pp. 1064–1082.
35. LANDAU, L. D.; AND LIFSHITZ, E. N. (E. PEIERLS AND R. F. PEIERLS, TRANS.): Statistical Physics. Addison-Wesley Pub. Co., 1958, p. 434.
36. MARGENAU, HENRY; AND MURPHY, GEORGE M.: The Mathematics of Physics and Chemistry. Second ed., D. Van Nostrand Co., Inc., 1956, ch. 6.
37. GOR'KOV, L. P.: Microscopic Derivation of the Ginzburg-Landau Equations in the Theory of Superconductivity. Soviet Phys.—JETP, vol. 9, no. 6, Dec. 1960, pp. 1364–1367.
38. ONSAGER, L.: Statistical Hydrodynamics. Nuovo Cim., vol. 6, Suppl. 2, 1949, pp. 279–287.
39. FEYNMAN, R. P.: Application of Quantum Mechanics to Liquid Helium. Progress in Low Temperature Physics. Vol. 1. C. J. Gorter, ed., Interscience Publ., 1955, pp. 17–53.
40. KLEINER, W. H.; ROTH, L. M.; AND AUTLER, S. H.: Bulk Solutions of Ginzburg-Landau Equations for Type II Superconductors: Upper Critical Field Region. Phys. Rev., vol. 133A, no. 5, Mar. 2, 1964, pp. 1226–1227.
41. MATRICON, J.: Energy and Elastic Moduli of a Lattice of Vortex Lines. Phys. Letters, vol. 9, no. 4, May 1, 1964, pp. 289–291.
42. DE GENNES, PIERRE G. (P. A. PINCUS, TRANS.): Superconductivity of Metals and Alloys. W. A. Benjamin, Inc., 1966, p. 73.
43. GOODMAN, B. B.: Superconductivity—The Structure of the Mixed State. Comp. Rend. Acad. Sci. Paris, vol. 258, no. 21, May 25, 1964, pp. 5175–5178.
44. JOINER, W. C. H.; AND BLAUGHER, R. D.: Magnetic and Resistive Transitions of Some Mo-Re Alloys. Rev. Mod. Phys., vol. 36, no. 1, pt. 1, Jan. 1964, pp. 67–69.

45. PINCUS, P.; GOSSARD, A. C.; JACCARINO, V.; AND WERNICK, J. H.: NMR Measurements of the Flux Distribution in Type II Superconductors. Phys. Letters, vol. 13, no. 1, Nov. 1, 1964, pp. 21–22.
46. CRIBIER, D.; ET AL.: Neutron Diffraction by Vortex Lines in Superconducting Niobium. Proceedings of the International Conference on Magnetism. Inst. Phys. and Phys. Soc. London, 1964, pp. 285–287.
47. CRIBIER, D.; JACROT, B.; MADHOV RAO, L.; AND FARNOUX, B.: Mise en Evidence par Diffraction de Neutrons d'Une Structure Periodique du Champ Magnetique Dans le Niobium Supraconductor. Phys. Letters, vol. 9, no. 2, Apr. 1, 1964, pp. 106–107.
48. ESSMANN, U.; AND TRÄUBLE, H.: The Direct Observation of Individual Flux Lines in Type II Superconductors. Phys. Letters, vol. 24A, no. 10, May 8, 1967, pp. 526–527.
49. GORTER, C. J.: Note of the Superconductivity of Alloys. Phys. Letters, vol. 1, no. 3, May 1, 1963, pp. 69–70.
50. KIM, Y. B.; HEMPSTEAD, C. F.; AND STRNAD, A. R.: Flux Creep in Hard Superconductors. Phys. Rev., vol. 131, no. 6, Sept. 15, 1963, pp. 2486–2495.
51. ANDERSON, P. W.: Theory of Flux Creep in Hard Superconductors. Phys. Rev. Letters, vol. 9, no. 7, Oct. 1, 1962, pp. 309–311.
52. DUNLAP, R. D.; HEMPSTEAD, C. F.; AND KIM, Y. B.: Magnetic Field Stabilization with a Superconducting Tube. J. Appl. Phys., vol. 34, no. 10, Oct. 1963, pp. 3147–3148.
53. KIM, Y. B.; HEMPSTEAD, C. F.; AND STRNAD, A. R.: Flux-Flow Resistance in Type-II Superconductors. Phys. Rev., vol. 139A, no. 4, Aug. 16, 1965, pp. 1163–1172.
54. STRNAD, A. R.; HEMPSTEAD, C. F.; AND KIM, Y. B.: Dissipative Mechanism in Type-II Superconductors. Phys. Rev. Letters, vol. 13, no 26. Dec. 28, 1964, pp. 794–797.
55. PEARL, J.: On the Nature of Resistance in the Mixed State of Type II Superconductors. Phys. Letters, vol. 17, no. 1, June 15, 1965, pp. 12–14.
56. PEARL, JUDEA: Direct Evidence of Steady EMF Induced by Flux Motion in Superconductors. Phys. Rev. Letters, vol. 16, no. 3, Jan. 17, 1966, pp. 99–100.
57. MEISSNER, HANS: Flux Flow Velocity in Superconducting Films by Measurement of Passage Time. Bull. Am. Phys. Soc., vol. 14, no. 1, Jan. 1969, p. 112.
58. GIAEVER, IVAR: Magnetic Coupling between Two Adjacent Type-II Superconductors. Phys. Rev. Letters, vol. 15, no. 21, Nov. 22, 1965, pp. 825–827.
59. GIAEVER, I.: Flux Pinning and Flux-Flow Resistivity in Magnetically Coupled Superconducting Films. Phys. Rev. Letters, vol. 16, no. 11, Mar. 14, 1966, pp. 460–462.
60. HEMPSTEAD, C. F.; AND KIM, Y. B.: Resistive Transitions and Surface Effects in Type-II Superconductors. Phys. Rev. Letters, vol. 12, no. 6, Feb., 10, 1964, pp. 145–148.
61. JONES, R. G.; RHODERICK, E. H., AND ROSE-INNES, A. C.: On the Origin of Resistance in the Mixed State of Type-II Superconductors. Phys. Letters, vol. 15, no. 3, Apr. 1, 1965, pp. 214–215.
62. LORCH, H. O.: On the Movement of Flux Lines in Type-II Superconductor. Phys. Letters, vol. 17, no. 3, July 15, 1965, pp. 196–197.
63. PARK, J. G.: On the Electric Fields in Flux Tubes and Current Vortices in Type 1 and Type 2 Superconductors. Phys. Letters, vol. 20, no. 4, Mar. 1, 1966, pp. 346–348.
64. JOSEPHSON, B. D.: Potential Differences in the Mixed State of Type-II Superconductors. Phys. Letters, vol. 16, no. 3, June 1, 1965, pp. 242–243.
65. GOODMAN, B. B.: The Electrodynamics of Flux Penetration in Superconductors. Phys. Letters, vol. 18, no. 1, Aug. 1, 1965, pp. 8–9.
66. JACKSON, JOHN D.: Classical Electrodynamics. John Wiley & Sons, Inc., 1962.
67. LANE, CECIL T.: Superfluid Physics. McGraw-Hill Book Co., Inc., 1962, p. 114.
68. BARDEEN, JOHN; AND STEPHEN, M. J.: Theory of the Motion of Vortices in Superconductors. Phys. Rev., vol. 140A, no. 4, Nov. 15, 1965, pp. 1197–1207.

69. MILLER, PIOTR B.: Frequency-Dependent Hall Effect in Normal and Superconducting Metals. Phys. Rev., vol. 121, no. 2, Jan. 15, 1961, pp. 435–450.
70. NOZIÈRES, P.; AND VINEN, W. F.: The Motion of Flux Lines in Type-II Superconductors. Phil. Mag., vol. 14, no. 130, Oct. 1966, pp. 667–688.
71. DE GENNES, P. G.; AND MATRICON, J.: Collective Modes of Vortex Lines in Superconductors of the Second Kind. Rev. Mod. Phys., vol. 36, no. 1, pt. 1, Jan. 1964, pp. 45–48.
72. NIESSEN, A. K.; AND STAAS, F. A.: Hall Effect Measurements on Type-II Superconductors. Phys. Letters, vol. 15, no. 1, Mar. 1, 1965, pp. 26–28.
73. HAKE, R. R.: Mixed-State Hall Effect in an Extreme Type-II Superconductor. Phys. Rev., vol. 168, no. 2, Apr. 10, 1968, pp. 442–444.
74. REED, W. A.; FAWCETT, E.; AND KIM, Y. B.: Observations of the Hall Effect in Superconductors. Phys. Letters, vol. 14, no. 19, May 10, 1965, pp. 790–792.
75. FIORY, A. T.; AND SERIN, B.: Influence of Oscillating Fields on the Hall Effect and Resistance of Superconducting Niobium. Phys. Letters, vol. 25A, no. 7, Oct. 9, 1967, pp. 557–558.
76. FIORY, A. T.; AND SERIN, B.: Resistivity and Hall Effect in Superconducting Nb. Phys. Rev. Letters, vol. 21, no. 6, Aug. 5, 1968, pp. 359–361.
77. MAXFIELD, B. W.: The Damping of Helicon Resonances in Pure Type-II Superconductors. Solid State Comm., vol. 5, no. 8, Aug. 1967, pp. 585–589.
78. ABRAMOWITZ, MILTON; AND STEGUN, IRENE A.: Handbook of Mathematical Functions with Formulas, Graphs, and Mathematical Tables. Appl. Math. Ser. 55, National Bureau of Standards, June 1964.
79. MAKI, K.: The Magnetic Properties of Superconducting Alloys. I. Physics, vol. 1, no. 1, July–Aug. 1964, pp. 21–30.
80. MAKI, K.: The Magnetic Properties of Superconducting Alloys. II. Physics, vol. 1, no. 2, Sept.–Oct. 1964, pp. 127–143.
81. VOLGER, J.; STAAS, F. A.; AND VAN VIJFEIJKEN, A. G.: Viscous Flow of Flux in a Pure Superconductor of the Second Kind. Phys. Letters, vol. 9, no. 4, May 1, 1964, pp. 303–304.
82. STEPHEN, M.; AND BARDEEN, J.: Viscosity of Type-II Superconductors. Phys. Rev. Letters, vol. 14, no. 4, Jan. 25, 1965, pp. 112–113.
83. TINKHAM, M.: Viscous Flow of Flux in Type-II Superconductors. Phys. Rev. Letters, vol. 13, no. 26, Dec. 28, 1964, pp. 804–807.
84. KUNZLER, J. E.; BUEHLER, E.; HSU, F. S. L.; AND WERNICK, J. H.: Superconductivity in Nb_3Sn at High Current Density in a Magnetic Field of 88 kgauss. Phys. Rev. Letters, vol. 6, no. 3, Feb. 1, 1961, pp. 89–91.
85. FRIEDEL, J.; GENNES, P. G. DE; AND MATRICON, J.: Nature of the Driving Force in Flux Creep Phenomena. Appl. Phys. Letters, vol. 2, no. 6, Mar. 15, 1963, pp. 119–121.
86. SILCOX, J.; AND ROLLINS, R. W.: Hysteresis in Hard Superconductors. Appl. Phys. Letters, vol. 2, no. 12, June 15, 1963, pp. 231–233.
87. LIVINGSTON, J. D.: Magnetic Properties of Superconducting Lead-Base Alloys. Phys. Rev., vol. 129, no. 5, Mar. 1, 1963, pp. 1943–1949.
88. SWARTZ, PAUL S.: Evidence for the Negative Surface Energy Models of Superconductivity in Nb_3Sn, Nb_3Al, V_3Ga, and V_3Si. Phys. Rev. Letters, vol. 9, no. 11, Dec. 1, 1962, pp. 448–451.
89. NARLIKAR, A. V.; AND DEW-HUGHES, D.: The Effect of Dislocation Configuration on the Superconducting Properties of Niobium and Vanadium. Phys. Stat. Sol., vol. 6, 1964, pp. 383–390.

90. WEBB, W. W.: Dislocations in Superconductors. Phys. Rev. Letters, vol. 11, no. 5, Sept. 1, 1963, pp. 191–193.
91. YAMAFUJI, K.; AND IRIE, F.: On the Concept of Pinning Force in Type-II Superconductors. Phys. Letters, vol. 25A, no. 5, Sept. 11, 1967, pp. 387–388.
92. LIVINGSTON, J. D.: Structure and Properties of High-Field Superconductors. Proceedings of the 1968 Summer Study on Superconducting Devices and Accelerators. Rep. BNL–50155, pt. 2, Brookhaven Nat. Lab., Apr. 1969, pp. 377–392.
93. STEPHEN, M. J.; AND SUHL, H.: Weak Time Dependence in Pure Superconductors. Phys. Rev. Letters, vol. 13, no. 26, Dec. 28, 1964, pp. 797–800.
94. SCHMID, A.: A Time Dependent Ginzburg-Landau Equation and Its Application to the Problem of Resistivity in the Mixed State. Phys. Kondens. Materie, vol. 5, no. 4, 1966, pp. 302–317.
95. BARDEEN, J.: Transport in Nonhomogeneous Superconductors. Paper presented at Meeting on Superconductivity, Stanford (California), Aug. 26–29, 1969.
96. TRÄUBLE, H.; AND ESSMANN, U.: Der direkte Nachweis von Flublinienbewegungen in Stromdurchflossenen Supraleitern. Phys. Stat. Sol., vol. 25, 1968, pp. 395–402.
97. TRÄUBLE, H.; AND ESSMANN, U.: Die Beobachtung magnetischer Strukturen von Supraleitern zweiter Art. Phys. Stat. Sol., vol. 20, 1967, pp. 95–111.
98. SARMA, N. V.: Transition from the Flux Lattice to the Intermediate State Structure in a Lead-Indium Alloy. Phil. Mag., vol. 18, no. 151, July 1968, pp. 171–176.
99. KRÄGELOH, U.: Flux Line Lattices in the Intermediate State of Superconductors with Ginzburg Landau Parameters near $1/\sqrt{2}$. Phys. Letters, vol. 28A, no. 9, Feb. 10, 1969, pp. 657–658.
100. ESSMANN, U.: Flux Flow and the Mixed State in Type-II Superconductors. Paper presented at Meeting on Superconductivity, Stanford (California), Aug. 26–29, 1969.
101. HUDSON, WAYNE R.; AND JIRBERG, RUSSELL J.: Nonlinear Flux Flow in Single Crystal Niobium. NASA TN D–5198, 1969.
102. SHOENBERG, DAVID: Superconductivity. Second ed., Cambridge Univ. Press, 1960.
103. FIETZ, WILLIAM A.: Reversible and Irreversible Magnetic Properties of Some Type 2 Alloy Superconductors. Ph. D. Thesis, Cornell Univ., 1967.
104. Anon.: RCA Rev., vol. 25, no. 3, Sept. 1964.

U.S. GOVERNMENT PRINTING OFFICE : 1970 OL—388–980

"The aeronautical and space activities of the United States shall be conducted so as to contribute . . . to the expansion of human knowledge of phenomena in the atmosphere and space. The Administration shall provide for the widest practicable and appropriate dissemination of information concerning its activities and the results thereof."

— NATIONAL AERONAUTICS AND SPACE ACT OF 1958

NASA SCIENTIFIC AND TECHNICAL PUBLICATIONS

TECHNICAL REPORTS: Scientific and technical information considered important, complete, and a lasting contribution to existing knowledge.

TECHNICAL NOTES: Information less broad in scope but nevertheless of importance as a contribution to existing knowledge.

TECHNICAL MEMORANDUMS: Information receiving limited distribution because of preliminary data, security classification, or other reasons.

CONTRACTOR REPORTS: Scientific and technical information generated under a NASA contract or grant and considered an important contribution to existing knowledge.

TECHNICAL TRANSLATIONS: Information published in a foreign language considered to merit NASA distribution in English.

SPECIAL PUBLICATIONS: Information derived from or of value to NASA activities. Publications include conference proceedings, monographs, data compilations, handbooks, sourcebooks, and special bibliographies.

TECHNOLOGY UTILIZATION PUBLICATIONS: Information on technology used by NASA that may be of particular interest in commercial and other non-aerospace applications. Publications include Tech Briefs, Technology Utilization Reports and Notes, and Technology Surveys.

Details on the availability of these publications may be obtained from:

SCIENTIFIC AND TECHNICAL INFORMATION DIVISION

NATIONAL AERONAUTICS AND SPACE ADMINISTRATION

Washington, D.C. 20546